The Circulatory System

<div style="text-align:right">**2**</div>

This chapter analyzes the macrocirculation, the microcirculation, and the lymphatic system of the vascular apparatus. We discuss the structure of the vessel wall, the main principles of hemodynamic control, and the mechanisms of vascular exchange. We look at the circulation from a system's perspective and introduce mechanical properties, such as pressure, capacity, flow, and vascular bed resistance. In addition, we explore the structure of the capillary wall toward the description of transcapillary transport mechanisms in microcirculation. The final part of this chapter introduces a number of lumped parameter models in the description of the macro- and microcirculation. In addition to WindKessel (WK) models, two and three-element models are derived toward the representation of vessel networks. Such models aim at capturing the steady-state, steady-periodic, and transient description of vasculature domains. With respect to microcirculation, hydrostatic and osmotic effects are examined, and vascular exchange is described by linear and nonlinear filtration models. Conclusions regarding the advantages and limitations of the discussed lumped-parameter models and future perspectives summarize this chapter.

2.1 Introduction

The evolution of species led to a more and more organized circulatory system. Simple diffusion of extracellular liquid evolved towards a highly *organized circulatory system* in mammals. This was made possible by the heart's pumping ability and regulated by peripheral resistances, which together generated the arterial blood

---

The original version of this chapter was revised: ESM has been added. The correction to this chapter is available at https://doi.org/10.1007/978-3-030-70966-2_8

T. C. Gasser, *Vascular Biomechanics*, https://doi.org/10.1007/978-3-030-70966-2_2

pressure and *flow*. Hemodynamics is therefore a fundamental organizing principle selected for diversification and adaptation of life.

The circulatory system is set up by two separate systems: the *cardiovascular system*, which distributes blood, and the *lymphatic system*, which collects lymph and returns it into the cardiovascular system, see Fig. 2.1. The cardiovascular system supplies blood to the body's organs and quickly adjusts to sudden changes in demand for oxygen, nutrients, and other factors in response to the organism's activity. The lymphatic system is open and essentially recycles blood plasma after it has been filtered from the *interstitial fluid*, the fluid situated between cells. Both systems cooperate in immune response.

The physiology and pathophysiology of the cardiovascular system have been extensively studied and excellent texts are available [394, 548]. The present chapter aims at introducing the topic to bioengineers, and the reader should then be able to understand and model key properties of the vascular system.

2.1.1   Vascular System

The vascular (or cardiovascular) system has three main functions:

- *Supply.* Distribution and exchange of oxygen, nutrients, and other substances
- *Cleaning.* Removal of waste products
- *Immune response.* Delivery of leucocytes to organs in response to pathogens, anything that can produce disease

In vertebras the cardiovascular system is closed and formed by the *systemic* and the *pulmonary* circuits, see Fig. 2.1. The systemic circulation transports oxygenated blood away from the left ventricle through the aorta to the rest of the body and then returns oxygen-depleted (deoxygenated) blood back to the right ventricle. Note that oxygen-depleted blood still contains approximately 75% of oxygen of oxygenated blood. The pulmonary circulation transports this blood through the lungs, where it is oxygenated. It then returns into the left ventricle and enters again the systemic circuit. Absolute values for oxygen consumption depend on body size, and young healthy humans at rest consume somewhere between 0.15 and 0.41 of oxygen per minute, a demand that can increase by 10 to 15 folds during exercise [288].

The essential components of the cardiovascular system are the heart, blood, and blood vessels. An average adult contains roughly 5.5 l of blood, accounting for approximately 7% of its total body weight. At rest, approximately 4 l min^{-1} or 80% of cardiac output is directed to the brain, heart, kidneys, and liver. Despite the cardiovascular system is closed, oxygen, nutrients, and macromolecules move across the wall of small blood vessels and enter the interstitial fluid on their way to the target cells. In return, carbon dioxide and wastes pass from the interstitial fluid directly back into small blood vessels, or through the lymphatic system back into the cardiovascular system. The transport of substances in and out of the vascular system is collectively called *exchange*.
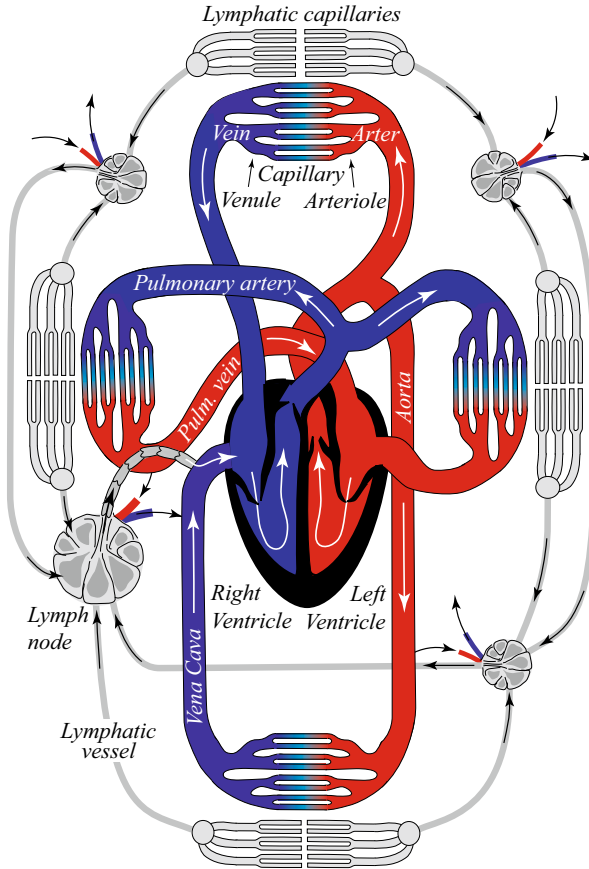
Fig. 2.1 The circulatory system comprises the cardiovascular system (systemic and pulmonary circuits) and the lymphatic system. *Systemic circuit:* The left ventricle pumps oxygenated blood through the aorta into all organs but the lungs. In the microcirculation blood is deoxygenated, and then the collected blood flows through the vena cava and returns into the right ventricle. *Pulmonary circuit:* The right ventricle pumps oxygen-depleted blood through the pulmonary artery into the lungs. In the microcirculation of the lungs, blood is oxygenated and returns through the pulmonary vein into the left ventricle. *Lymphatic system:* A one-way low-resistance network of drainage channels (lymphatic capillaries) returns lymph from the interstitial to lymph nodes and then, through the lymphatic venous anastomosis, into the venous system

The vascular system can also be seen to function in two parts: a *macrocirculation* and a *microcirculation*.

2.1.2 Key Concepts

Although the cardiovascular system shows large anatomical variability across species, key concepts are preserved. Some of these concepts are discussed in the following.

2.1.2.1 Form Follows Function

Given normal conditions, the cardiovascular system *continuously adapts* towards optimal system performance. The system is then at *homeostasis* and remains stable in time. Homeostasis is an essential component of biological evolution [552], and Cannon[1] [66] describes this biological system property as the following:

> The highly developed living being is an open system having many relations to its surroundings. Changes in the surroundings excite reactions in this system, or affect it directly, so that internal disturbances of the system are produced. Such disturbances are normally kept within narrow limits, because automatic adjustments within the system are brought into action and thereby wide oscillations are prevented and the internal conditions are held fairly constant.

Mechanical stress also excites vascular tissue reactions and explains a number of properties of the vascular system. The blood pressure in the systemic circuit is *much higher* than in the pulmonary circuit, and the left ventricle is therefore more muscular and has a thicker wall than the right ventricle. For the same reason the wall of arteries is thicker than of veins. The blood pressure determines the tension in the vessel wall, and the circumferential [91,363,598] and axial [215] *tensile force* in the vessel wall correlate with its thickness. Aside from pressure-related adaption, the diameter of blood vessels also adjusts to the blood flow in the vessel. The blood flows over the endothelium and induces *Wall Shear Stress (WSS)*, a quantity that is kept constant by adjusting the vessel's diameter [74,236].

The cardiovascular system uses a wide range of actions towards reaching homeostatic targets. We may group them into four classes of mechanisms:

- *Passive response.* Purely passive deformation under the action of forces
- *Vasoreactivity.* Vasoconstriction or vasodilation due to the action or relaxation of contractile cells in the vessel wall
- *Arteriogenesis.* Increase or decrease of the vessel's diameter and wall thickness in response to the turnover of tissue constituents
- *Angiogenesis.* Formation of new vessels sprouting out from pre-existing vessels

These adaptation mechanisms are linked to characteristic *time scales* and allow the system to adjust quickly (passive response) or very slowly (angiogenesis) towards meeting system needs. Whilst the aforementioned mechanisms are local, they have distinct system-level, and thus global implications. The homogenization of WSS would be one such example. It requires the total cross-sectional area of the vasculature to increase from the aortic cross-section of 3 to $5\,cm^2$ to the total cross-section of the capillary bed of 4500 to $6000\,cm^2$. Such a configuration of the vascular tree is energy-efficient and keeps the blood pressure relatively low in the systemic circuit.

---

[1]Walter Bradford Cannon, American physiologist, 1871–1945.

2.1.2.2 Blood Flows in Closed Loops

The vascular system is closed and local alterations have global implications—blood flowing through one organ affects the flow through another organ. Likewise, the pulmonary circulation influences the systemic circulation and *vice versa*, and the venous flow influences the arterial flow and *vice versa*.

The vascular system may also be divided into sub-loops with dedicated organ-supply function, which is most clearly observed in the kidney, the heart, and the brain. The pressure and flow within such sub-loops are separately controlled, a mechanism known as *autoregulation*, and allows for the (partly) independent operation of organs. The formation of sub-loops also explains the anatomical organization of the vascular tree with arteries and (deep) veins often running in parallel, and in close proximity to each other.

2.1.2.3 Vascular Network Is "Space Filling"

Only a very few tissues in mammals, such as the ligaments, the valve leaflets, and the cornea, are *avascular* and do not contain blood vessels. They are entirely perfused by *diffusion*. All other tissues contain vessels, with the vascular network being "space filling". Given limited resolutions, most of the vasculature remains invisible to *image modalities*, such as Computed Tomography (CT), Magnetic Resonance (MR), and ultrasound.

2.1.3   Cells in the Vascular System

The vascular system performs many very different tasks, such as transport and exchange, immune response, regulation of pressure and flow, Extra Cellular Matrix (ECM) maintenance, and the control of blood clotting and wound healing. These functions are carried out by *cells* together with their delicate interactions with ECM and blood plasma. Cells of the same type often perform multiple tasks to achieve proper system function.

2.1.3.1 Endothelium Cell

Endothelium Cells (ECs) are joined together to form a single-cell layer (monolayer) called *endothelium* that provides a clear separation between the blood and the vessel wall. ECs are flat and 0.2 to 2 μm thick. Given exposure to laminar blood flow, they align with the flow within 12 to 14 days [162] and adapt towards an elongated shape. The length of ECs ranges then from 1 to 20 μm. In humans, ECs make up approximately 1.0 kg and cover a surface of approximately 7000 m^2. ECs in arteries, capillaries, veins, and lymphatics are exposed to markedly different hemodynamic environments and must perform distant functions.

ECs sense WSS, in response to which they secrete vasoactive agents that control the tonus of adjacent contractile vascular cells, such as SMCs and pericytes. ECs also play a crucial role in response to inflammation. They express adhesion molecules towards capturing circulating leukocytes and promoting their transport into the tissue. ECs are also involved in immune response and tissue remodeling.

In their vicinity, ECs prevent blood from clotting by secreting vasoactive agents. In capillaries, ECs form a semipermeable membrane to allow oxygen, nutrients, and other factors to move into peripheral tissues whilst retaining blood cells and plasma in the circulation.

2.1.3.2 Smooth Muscle Cell

Smooth Muscle Cells (SMCs) can present either at the *contractile phenotype* or the *synthetic phenotype*. At the contractile phenotype, SMC serves as a contractile cell of arteries, arteriole, and veins. They appear at a spindle-shaped configuration, measuring approximately 2 to 5 µm in diameter and 100 to 500 µm in length. At the synthetic phenotype, the SMC synthesizes ECM proteins and has a more cobblestone-type shape. The cell appears then less elongated than at the contractile phenotype. In the vessel wall, SMCs are mainly aligned in circumferential vessel direction and communicate with each other though *tight junctions* and *gap junctions*.

2.1.3.3 Pericyte

Pericytes are the *contractile* cells of capillaries and venules. They regulate capillary blood flow and, together with ECs, the permeability of the vessel wall. Communication between pericytes and ECs is facilitated by *integrins*. Pericytes appear at an elongated shape of approximately 5 to 10 µm in length.

2.1.3.4 FibroBlast

FibroBlast (FB) *synthesizes ECM proteins*, out of which collagen is the most important one. FBs are 10 to 15 µm large and have a branched cytoplasm surrounding an elliptical nucleus. Active FBs have abundant rough endoplasmic reticulum, whereas inactive FBs, also denoted fibrocyte, appear more spindle-shaped. The active FB is attached to collagen fibers and puts them under tension—it pulls on collagen fibers. Given crowded FBs, they are often locally aligned in parallel clusters.

2.1.3.5 Erythrocyte

Erythrocytes (or red blood cells) are the most common type of blood cells, constituting almost half of the volume of blood. Their principal aim is to *deliver oxygen*. Erythrocytes have no nucleus, and they are highly deformable bi-concave-shaped discs, measuring approximately 6 to 8 µm in diameter and 2 to 4 µm in height.

2.1.3.6 Leukocyte

Leukocytes (or white blood cells) are cells of the *immune system* that are involved in protecting the body against infectious disease and foreign invaders. Leukocytes present in very different types, such as plasma cells, lymphocytes, and macrophages.

Plasma cells secrete large volumes of antibodies. They produce *antibody molecules* that bind to foreign substance (target antigen) and initiate its neutralization or destruction. They are 12 to 15 µm large, ovoid-shaped, and transported in blood plasma as well as in lymph. *Lymphocytes* are the main type of cell found in lymph and include natural killer cells, T cells, and B cells. They

are approximately 6 to 30 μm large. *Macrophages* engulf and digest pathogen, participate in the initiation and resolution of inflammation, and in the maintenance of tissues. They are approximately 20 μm in diameter and show very different shapes, adapted to the functions to be carried out.

2.1.3.7 Platelets

Platelets (or thrombocytes) are tiny blood cells, which together with coagulation factors, stop bleeding by *forming a blood clot*. They have no nucleus, and non-activated platelets are approximately 2 μm large and of compact shape. On activation, platelets turn into octopus-like shapes, with multiple arms and legs. Minutes after activation, platelets start aggregating with each other and/or depositing on surfaces that are not covered by ECs.

2.1.3.8 Dendritic Cell

Dendritic cells process antigen material and present it on the cell surface to the T cells of the immune system. Dendritic cells are 10 to 15 μm large and have a very large surface-to-volume ratio.

2.1.4 Macrocirculation

The macrocirculation *transports* blood through the cardiovascular system. The *systemic circuit* carries it through all organs, but the lungs, and the *pulmonary circuit* through the lungs.

The first part of the systemic circulation is the *aorta*, a massive and thick-walled artery that origins at the aortic valve. It then arches and gives branches supplying the upper part of the body. After passing through the aortic opening of the diaphragm, it enters the abdomen and supplies branches to abdomen, pelvis, perineum, and the lower limbs. The renal circulation by itself is supplied with approximately 20% of the cardiac output.

Along the vascular tree, the arterial lumen continuously decreases until blood flows though arterioles and passes capillaries, where the *exchange* of oxygen, nutrients, and other substances takes place. Capillaries are often organized in a *capillary bed*, an interweaving network of capillaries supplying tissues and organs. The blood is then collected by venules, before veins return it to the heart, see Fig. 2.1. The properties of the different types of blood vessels are adapted to their function:

- An *artery* carries blood away from the heart. The luminal diameter ranges up to centimeters and the thick wall is designed to cope with high blood pressure.
- An *arteriole* connects arteries to capillaries. The lumen is approximately 10 to 100 μm in diameter, and vasoreactivity (vasoconstriction or vasodilation) allows it to control the blood flow into the capillaries.
- A *capillary* has a luminal diameter of approximately 5 to 8 μm, just wide enough to allow erythrocytes passing/squeezing through. The wall is permeable and

allows the capillary to supply tissues with factors, such as oxygen and nutrients, and to remove waste products in return.

- A *venule* connects capillaries to veins and has a luminal diameter of approximately 10 to 200 μm. The wall is thinner than of arterioles and equipped with a highly permeable endothelium layer.
- A *vein* carries blood to the heart. The wall shows a thin media and a thick adventitia. Veins have a diameter that ranges up to centimeters and they are often larger than arteries.

The blood flow velocity changes by *four* orders of magnitudes along the arterial tree. In large arteries the blood shows phases of *forward and backward* flow at velocities of tens of centimeters per second, whilst the blood flow in capillaries is *unidirectional* and of tens of micrometers per second. In veins the blood flow is generally more uniform than in arteries, a condition partly supported by *valves*. Given limb veins, valves counteract gravitation and prevent from back flow. Blood flow velocities in the systemic and pulmonary circuits are similar.

In addition to the transport function of the macrocirculation, the *elasticity* of the large blood vessel is of fundamental importance to the proper physiological function of the cardiovascular system. Especially the aorta contributes almost the entire *volume compliance* to the cardiovascular system. Veins are much more distensible than arteries, which allows them to serve as *venous compartment*. Approximately 60% of the blood is stored in the veins, a compartment controlled by the autonomous nervous system.

2.1.4.1 Blood Vessel Structure and Function

Blood vessels are *distensible*, a key feature to lower the pulse pressure and to support continuous flow into the distal tissue. The distensibility is a consequence of the wall's elasticity. It is determined by the ECM through the delicate interaction of structures, such as elastin, collagen, ProteoGlycans (PGs), fibronectin, and fibrillin. Whilst the ECM determines the vessel wall's structural integrity, cells maintain its vasoreactivity, metabolism, and immune response. Vascular cells are also able to alter the elasticity of the vessel wall. Contractile cells can augment vessel wall properties within seconds, whilst the effect from newly synthesized ECM appears at a delay of weeks.

The wall of arteries, arterioles, veins, and venules is built up by *three* distinct vessel wall layers: intima, media, and adventitia, see Fig. 2.2. In contrast to larger vessels, the glycocalyx, the endothelium, and a basal membrane form the single-layered wall of capillaries. The structure of veins and arteries is very similar. Given the low pressure in the venous system, veins have a thinner wall than arteries. They may also be equipped with passive valves to prevent the back flow of blood.

2.1.4.2 The Intima and the Endothelium

The interaction of the glycocalyx, the endothelium (a monolayer of EC), and a subendothelial layer forms the *intima*. The glycocalyx binds different anti-inflammatory and anti-coagulant factors, and its disruption results in thrombin
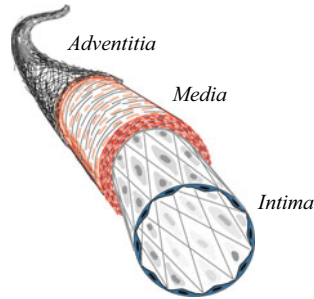
Fig. 2.2 The layered structure of large blood vessels. The adventitia is a collagen-rich fibrous layer that shields the inner layers from excessive mechanical forces and anchors the vessel to its surrounding. The media is a Smooth Muscle Cell (SMC)-rich layer that determines the physiological properties of large elastic vessels. The media is designed to withstand mechanical load acting along the circumference. The intima is dominated by a single layer of Endothelial Cells (ECs) that forms a lining between blood and tissue. The intima has important barrier functions

generation and platelet adhesion. The glycocalyx contributes also to EC mechanotransduction, and thus to the transduction of biomechanical forces into the biomolecular response of EC. Loss of glycocalyx apparently contributes to impaired sensing and transduction of WSS.

The endothelium provides an anti-thrombogenic and low-resistance lining between the blood and the vessel wall tissue. It responds to WSS and produces a host of chemical substances, such as Nitric Oxide (NO), endothelin, prostacyclin (PGI_2), and angiotensinogen, all are designed to maintain vascular homeostasis [394]. They modify the ability of platelets to adhere to the vascular wall and to aggregate with the formation of a blood clot. The endothelium is also a selective barrier for substances such as oxygen, nutrients, leukocytes, lipoproteins and influences factors, such as vessel wall permeability, tonus of contractile cells, inflammation, blood clotting, and tissue remodeling.

2.1.4.3 The Media

The *media* contains 30 to 60% vascular SMCs that are embedded in the ECM. The media's ECM itself contains 5 to 25% elastin, 15 to 40% collagen, and 15 to 25% other connective tissue. The media is formed by *Medial Lamellar Units (MLU)*, a structure that is clearly visible in elastic arteries but disappears towards muscular arteries. Elastic arteries are rich on elastin and found at the beginning of the vascular tree, whilst muscular arteries contain a large amount of vascular SMC and appear downwards the vascular tree. The media is the dominating layer in large elastic arteries and of utmost physiological relevance to the proper function of the cardiovascular system. The media is designed to cope with stress primarily along its circumferential direction.

   SMC in the media are specialized in tonic contraction (contractile phenotype) but also in the production of ECM constituents (synthetic phenotype). SMC tonus is controlled by the autonomous nervous system and regulates blood flow through vasoreactivity in response to the body's activity. The cells in the inner media (mainly SMCs) are entirely fed through *transmural flow*, fluid flow that establishes from the pressure differences in the lumen and the interstitial space. SMCs also participate in inflammatory reactions by modulating vascular tone, but they have a limited capacity in direct immune response.

2.1.4.4 The Adventitia

The *adventitia* is an ECM-rich layer with collagen fibers covering approximately 60 to 80% of its volume. Another 10 to 25% is occupied by other connective tissue components. In addition to numerous macrophages providing immune response, FB is the primary cell type found in the adventitia. It maintains the ECM and covers approximately 10% of the adventitia's volume. Tiny blood vessels, the *vasa vasorum*, perfuse the adventitia together with the outer media and deliver cells, such as leucocytes for immune response. The adventitia anchors blood vessels to surrounding tissues, and its dense mesh of collagen protects the biologically vital medial and intimal layers from overextension. The adventitia is penetrated by nerves that control the SMCs in the media, and it is often thinner in veins than arteries.

2.1.4.5 Wall Shear Stress (WSS)

NO has an important signaling function in the vessel wall. It is produced from L-arginine by activity of endothelial nitric oxide synthase (eNOS), an enzyme that is continually released from healthy EC. After the diffusion of NO into the media, it relaxes SMCs and maintains vascular patency and distensibility. Stimuli for the release of NO from EC include WSS, exerted directly on the EC membrane or on the endothelial layer [398], see Fig. 2.3. The expression of NO is also influenced by the blood flow conditions, and thus the temporal occurrence of the WSS, see Fig. 2.3b. Periodic flow stimulates greatly NO expression, whilst turbulent flow shows similar expression to static conditions.

   Aside from regulating the arterial diameter through the production of vasoactive mediators, WSS is also an important determinant of endothelial gene expression [394]. WSS regulates factors, such as transcription factors, growth factors, adhesion molecules, and enzymes. Endothelium function is optimal during youth and the absence of cardiovascular disease. With age endothelial function progressively deteriorates, which is then associated with the reduction of the bio-availability of NO and anatomical changes, such as thickening of the endothelia layer. The most obvious disfunction of the endothelium is seen with age-related diseases, such as atherosclerosis [394]. Endothelium function is defective, not only in patients with developed atherosclerosis, but already in persons with risk factors for atherosclerosis [557].

Fig. 2.3 Expression of Nitric
Oxide (NO) in relation to the
Wall Shear Stress (WSS) that
is applied to the membrane of
Endothelial Cells (ECs) (**a**) or
at the endothelial layer (**b**).
NO expression is illustrated
through the formation of [^{3}H]
L-citrulline, a by-product of
NO expression

(a)

(b)
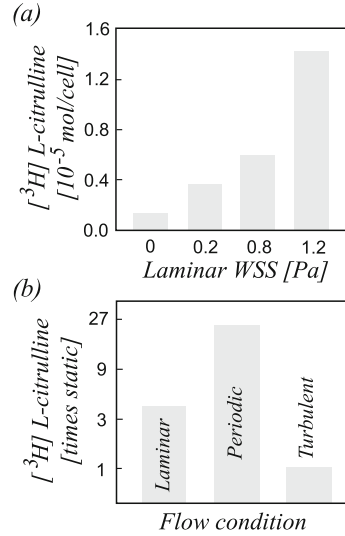
2.1.5 Lymphatic System

The lymphatic system constitutes a *one-way* low-resistance network of drainage
channels that operates in conjunction with the cardiovascular system and returns
lymph from the interstitial to the venous system, see Fig. 2.1. It plays a major
role in helping the *immune system* to defend the body against diseases and serves
as a "highway" for fast and efficient delivery of immune cells, as well as free
antigens [63]. In a healthy human, lymph flow of approximately eight liters per
day is expected, from which approximately half can be absorbed by lymph node
microvessels, leaving four liters per day post-nodal lymph flow left.

The lymphatic system is composed of lymphatic vessels and lymphoid organs,
such as the bone marrow, thymus, lymph nodes, spleen, Peyer's[2] patches, tonsils,
and the appendix. Lymph flow is unidirectional and establishes through the rhythmic
contraction of lymphatic contractile cells. Skeleton muscle contractions and arterial
pulsations support the synchronized opening and closing of intra-luminal lymphatic
valves—the *lymph propulsion*. In addition to nerves and chemicals, mechanical
factors, such as the streamwise pressure gradient, transmural pressure, preload and
afterload influence lymph propulsion.

Lymphatic vessels are *absorptive* vessels and found in almost all organs—
recently they have also been identified in the brain [3]. Lymph nodes are located
at the intersections of collecting lymphatics. Lymph nodes filter the interstitial
flow and break down bacteria, viruses, and waste. Under normal conditions,
interstitial fluid pressure is below atmospheric pressure whilst fluid in lymphatic

---

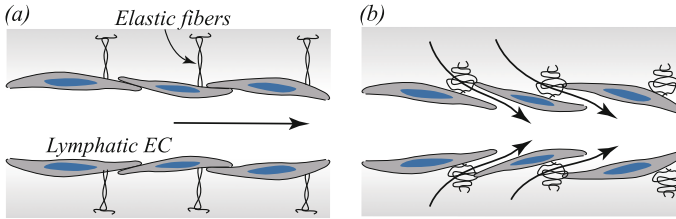[2]Johann Conrad Peyer, Swiss anatomist, 1653–1712.

Fig. 2.4 Functioning of primary valves of lymphatics capillaries. Vessel configurations at low (**a**) and high (**b**) interstitial pressures. Arrows indicate fluid flow

capillaries is slightly above atmospheric pressure. Intra-lymphatic pressure slowly *increases* along the drainage route, and thus towards the larger collecting vessels and ultimately the thoracic duct or right lymphatic trunk, where lymph is returned to the blood circulation. Lymph propulsion establishes flow therefore against a positive streamwise pressure gradient.

The biomechanics of the lymphatic system are not yet very well explored, and further details, including its modeling, are reported elsewhere [285, 355, 454].

2.1.5.1 Lymphatic Vessels

Lymphatics *capillaries* are approximately 10 to 60 μm in diameter. A single layer of partially overlapping lymphatic EC forms their approximately 50 to 100 nm thick wall, see Fig. 2.4. Whilst it has neither a basal lamina nor contractile cells, it is equipped with active valves, so-called *primary valves*, to collect interstitial fluid. The lymphatic EC are oak-leaf-shaped and joined together by "button-like" junctions to form such primary valves. The lymphatic ECs are also anchored to the surrounding ECM through elastic fibers that function as mechanosensors. The fibers detect increased tissue pressure and open the primary valves to allow interstitial fluid to enter, see Fig. 2.4. Once the surrounding tissue swells, the primary valves open and fluid, macromolecules, and immune cells enter the lymphatic capillary.

The pre-collecting lymphatics connect the capillaries to the collecting lymphatics. Collecting lymphatics have diameters of 1 to 2 mm, contain intra-luminal valves, and their ECs are highly interconnected. Similar to blood vessels, the wall of collecting lymphatics is formed by three distinct wall layers: *intima, media*, and *adventitia*.

As with blood vessels, lymphatics adjust in response to mechanical and biochemical stimuli [189]. NO [190], histamine [396], and endothelin [484] are known to influence lymphatic contractility. Lymph flow is complex and corresponds to conditions of no flow, slow flow, and retrograde flow. The endothelium is therefore exposed to a wide range of WSS, and endothelial-derived NO is expected to have an important role in the orchestrated propulsion of the lymphatic system [127, 128].

2.1.6 Microcirculation

Organs are perfused by *feed arteries* that branch off a major conduit artery. Four to six branch orders are then counted before the terminal arterioles give rise to capillaries, where the *exchange* with the interstitial tissue appears.

Arterioles, capillaries, and venules regulate vascular *pressure* and *divert* blood flow to meet local metabolic needs. Their diameters are controlled by the tonus of pericytes, which in turn determine the pressure drop along these vessels. It is the arterioles that play a major role in the distribution of blood towards the most metabolically stressed areas. In contracting skeletal muscles, for example, marked dilation is seen in the smallest arterioles [562], whilst approximately 80% of capillaries are perfused at rest.

Delicate alterations in the capillary "forces" and vessel properties determine fluid exchange characteristics and allow for moment-to-moment regulation of *transcapillary fluid flow*, a mechanism knows as *filtration*. Whilst diffusion determines the transport of the small molecules, filtration controls the advection of large solutes. The permeability of capillaries to water and solutes is often regarded constant, but this property is known to change at least in response to volume regulatory hormones and WSS that is sensed by ECs [307, 347].

Aside from exchange, the microvasculature restores blood pressure towards normal levels and serves as an autotransfusion compartment—at vascular volume overload fluid it automatically removed from the bloodstream and *vice versa*.

2.1.6.1 Exchange

Any factor in the blood that will be delivered from the capillary into the tissue has to *pass* the vascular wall, formed by the glycocalyx, endothelium, and basal membrane. This structure is adapted to support molecular exchange. Transport of liquid and solutes between the intravascular space and the interstitium, and thus across the semipermeable vascular endothelial barrier, is accomplished by:

- *Diffusion.* Transport of a substance down its concentration gradient. It is the primary mechanism for oxygen and lipids, and partial mechanism for proteins.
- *Advection.* Transport of a substance together with bulk motion of water and determined by gradients of hydrostatic and osmotic pressures. It is the primary mechanism for water and ions, and the partial transport mechanism for proteins.
- *Transcytosis.* Macromolecules, such as proteins, are captured in vesicles on one side of the EC, drawn across the cell, and ejected on the other side.

Under normal conditions, the balance of "forces" acting across the walls of exchange vessels favors the net flux of fluid *from the bloodstream to the interstitium*, a process commonly referred to as *capillary filtration*. Based on Starling's[3] equation (see Sect. 2.4.2), it has been estimated that in a healthy human, approximately

---

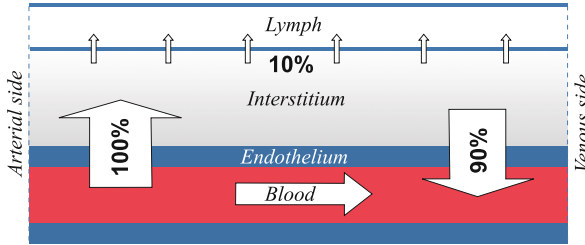[3]Ernest Henry Starling, British physiologist, 1866–1927.

Fig. 2.5 Historical understanding of microcirculatory fluid fluxes between vascular (red), interstitial (gray), and lymphatic (white) spaces. More recent data suggests much less reabsorption back into the vascular space in some tissues, and much more fluid is then transferred into the lymphatic system

90% of the fluid that moves from the vascular capillaries into the interstitium will be *reabsorbed* back into the vascular system, whereas 10% will move into the lymphatic system, see Fig. 2.5. This quantification has been proposed by Starling in 1896 [524] and provided useful insights in vascular exchange. However, it also failed to explain some experimental observations [338], and additional experimental data [371] indicated much less reabsorbtion back into the vascular capillary. We may therefore conclude that the drainage of capillary filtrate by the lymphatic system is another dominating factor in interstitial volume homeostasis [338].

2.1.6.2 Colloid Osmotic Pressure and the Role of Albumin

Osmosis is the spontaneous flow of a solvent across a semipermeable membrane *towards* a more concentrated solution, see Appendix E.2. Osmotic pressure is the pressure that must be applied to the side of the more concentrated solution to stop such a flow. In the vasculature, the solvent is water, and solutes are typically macromolecules. The osmotic pressure usually tends to pull water *into* the vascular system, and as such opposes the hydrostatic pressure pushing water through the capillary wall *out* of the vascular system.

The *Colloid Osmotic Pressure (COP)*, or oncotic pressure, is the osmotic pressure exerted by proteins and largely determined by the concentration of *albumin*. The total COP of an average capillary is approximately 28 mmHg with albumin contributing approximately 22 mmHg. Albumin is produced in the liver. It is the most abundant blood plasma protein and constitutes approximately 50% of human plasma proteins. It is essential for maintaining COP, and as such responsible for proper distribution of body fluids between blood vessels and body tissues. With approximately 10 nm in diameter, albumin is smaller than most other proteins, which allows it to pass the capillary wall relatively easy. Therefore, approximately 50 to 60% of albumin content resides in the interstitium at an average concentration of approximately 15 g l^{-1}. In adipose tissue concentrations of 4.3 to 10.7 g l^{-1}, and in skeletal muscle 9.7 to 15.7 g l^{-1} have been reported [138]. In addition, glycosaminoglycans (GAGs) and collagen exclude albumin from up to 50% of interstitial space, such that local albumin concentration approaches 20 to 30 g l^{-1}

in the interstitium. This is approximately half of 35 to 50 g l^{-1}, the albumin concentration seen in the capillary lumen [40].

Besides controlling COP, albumin transports a wide variety of substances, such as fatty acids, calcium, phospholipids, bilirubin, enzymes, hormones, drugs, metabolites, and ions. Like other proteins in the interstitial spaces, albumin returns to the circulation via lymph.

2.1.6.3 Functional Adaptation of Capillaries

Regardless of capillaries being the smallest vessels, they have the *highest cumulative surface area* available for exchange. Exchange of oxygen occurs primarily from erythrocyte "packets" as they pass through the vessel, whilst CO, fluids, and molecules up to the size of the plasma proteins are exchanged directly between plasma and the interstitial space. Given the different exchange functions, capillaries may be classified as *continuous, fenestrated*, and *discontinuous*, see Fig. 2.6.

Continuous capillaries have a low hydraulic conductivity and feature strong barriers between blood and tissue. The tightest continuous capillaries form barriers known as the Blood–Brain Barrier (BBB), the Blood–Aqueous Barrier (BAB), the Blood–Nerve Barrier (BNB), and the blood–testes barrier. Such barriers involves the formation of specialized adherens and tight junctional structures between adjacent ECs. Given the BBB, it features transcytosis by specialized transporters to facilitate one-way and selective movement of the glucose and other small solutes. Pathological changes of the BBB are associated with stroke, Central Nervous System (CNS) inflammation, and neuropathologies including Alzheimer's disease, Parkinson's disease, epilepsy, multiple sclerosis, and brain tumors.

Fenestrated capillaries are equipped with fenestrae of the size of 20 to 100 nm that penetrate the endothelium and conduct fluid with considerable ease. Fenestrated capillaries are found in the kidney, area postrema, carotid body, endocrine and

Fig. 2.6 Types of capillaries. (**a**) Continuous capillaries have a continuous endothelium and a continuous basal membrane. Endothelial cells (ECs) are connected via tight junctions. (**b**) Fenestrated capillaries display endothelium with fenestrae on top of a continuous basal membrane. (**c**) Discontinuous capillaries are larger than the other capillaries and show large fenestrae and a fragmented basal membrane

(a) Continuous Capillary

Continuous Basal Lamina

Tight Junction

(c) Discontinuous Capillary

Large Fenestrae

(b) Fenestrated Capillary

Fenestrae

Continuous Basal Lamina

Discontinuous Basal Lamina
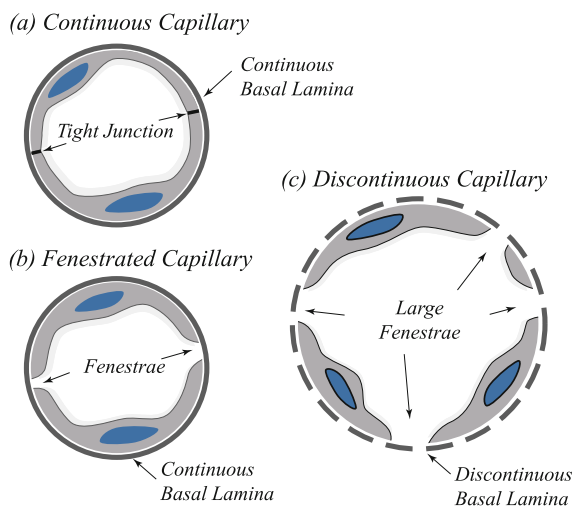
exocrine pancreas, thyroid, adrenal cortex, pituitary, choroid plexus, small intestinal villi, joint capsules, and epididymal adipose tissue.

Discontinuous capillaries show wide spacing between ECs, ranging up to micrometers, on top of a fenestrated basal membrane. Discontinuous capillaries have a very high hydraulic conductivity and are found in organs involved in the sequestration of formed vascular cells, such as spleen, bone marrow, or in the synthesis and degradation of fats and proteins, such as the liver.

2.1.6.4 The Glycocalyx

Fig. 2.7 illustrates the *glycocalyx*, a layer that plays a central role as physical barrier at the blood–endothelial interface. It is a negatively charged polysaccharide-rich surface layer that covers the luminal side of the endothelium. The glycocalyx is approximately one micrometer thick; in electron microscopy its thickness appears 50 to 300 nm and in confocal microscopy 2.5 to 4.5 µm. The glycocalyx layer is the first barrier that is permeable to water and solutes, such as electrolytes and small molecules. However, it prevents erythrocytes from contact with the EC surface and retains plasma proteins and inflammatory leukocytes in the vascular space, before any trans- or paracellular transfers appear. In continuous capillaries, the filtration of species is tightly controlled by the glycocalyx layer, and its interpolymer spaces function as a system of small pores with radii of approximately 5 nm. Given fenestrated and discontinuous capillaries, fenestrae provide an additional pathway for solvent and solutes, see Fig. 2.6.

2.1.6.5 Controlling Blood Pressure and the Role of Resistance Vessels

The small diameters of arterioles, capillaries, and venules poses considerable resistance to blood flow—they are therefore also called *resistance vessels*. Resistance vessels are highly vasoreactive, and the tonus of the pericytes in their walls controls their diameters, a mechanism to maintain an almost constant system pressure. During heavy exercise cardiac output is increasing four- to eightfold, whilst the Mean Arterial Pressure (MAP) rises by about 15 to 20 mmHg, and thus by less than 20% [366].

The resistance vessels are able to divert bloodstreams, an observation already reported in the late 1700s by Hunter:[4] *"blood goes to where it is needed"*. Given a local need of blood supply, the diameter of the local resistance vessels is controlled in response to the *metabolic tension* of the surrounding tissue. At heavy exercise up

Fig. 2.7 Schematic illustration of the glycocalyx layer, a barrier at the blood-endothelial interface

---
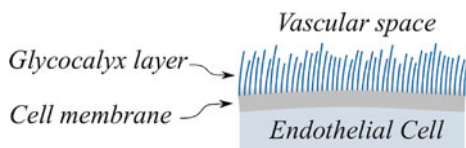
[4]William Hunter, Scottish anatomist and physician, 1718–1783.

to two liters of blood flow can be redirected to the skeletal muscles [288]. Given the onset of muscle contraction, vasodilation in the muscle microcirculation is delayed by only 5 to 20 s [359].

Whilst MAP increases only slightly during exercise, pulse pressure can increase dramatically. The peripheral vasodilation reduces the diastolic pressure, and the larger blood volume ejected by the left ventricle increases the systolic pressure [477], both of which contributes to the pulse pressure increase.

2.1.7   Hemodynamic Regulation

Hemodynamic regulation aims at maintaining the local equilibrium between delivery and consumption of blood-borne substances. Blood flow distribution through the vascular system can either be controlled by the CNS, or locally through neural impulses and hormonal cues. The endothelium, a semipermeable barrier sitting at the strategic position between blood and wall, plays a central role and responds to mechanical as well as chemical signals.

The tonus of contractile cells allows for the control of the vessel's diameter and thus the local delivery of blood to the tissue. At the physiological tonus, the vessel has its physiological diameter, which may be increased or decreased through the expression of *vasodilators* and *vasoconstrictors*, respectively. Whilst NO is a dominant vasodilator in large arteries, endothelium-driven hyperpolarization factors (EDHF), such as hydrogen peroxide, epoxyeicosatrienoic acids, prostacyclin, prostaglandin, and others contribute to the dilation of resistance vessels. The concentration of vasoconstrictors, such as catecholamines, Atrial Natriuretic Peptide (ANP), vasopressin, bradykinin, also affects the status of contractile vascular cells. Many of these factors may also influence EC's release of NO, and the net effect from vasodilators and vasoconstrictors determines the final vessel diameter.

2.1.7.1 Autoregulation Mechanisms

Hemodynamic regulation establishes at different levels, and individual vascular regions are regulated autonomously from other parts of the vascular system.

Given *myogenic regulation*, the vessel dilates or constricts in response to changing intravascular pressure [282, 498]. An elevated pressure causes paradoxically vasoconstriction and augments the arterial resistance. This mechanism enables matching blood supply to tissue demand over the pressure range of approximately 8 to 20 kPa. Myogenic regulation is mediated by contractile vascular cells and independent from ECs. A pressure increase in most resistance arteries involves stretch-induced activation of nonselective cation channels. This activation causes cell membrane depolarization, calcium influx, and cell contraction. The *Bayliss*[5] *effect* is a special example of myogenic regulation of arterioles, see Fig. 2.8.

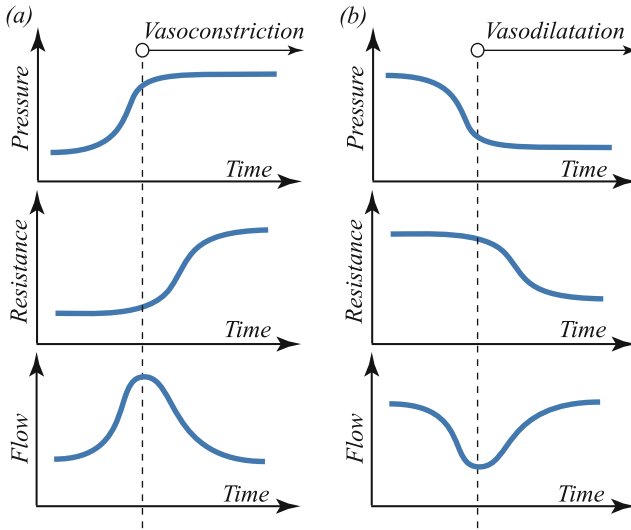[5]Sir William Maddock Bayliss, English physiologist, 1860–1924.

Fig. 2.8 The Bayliss effect is a particular myogenic regulation mechanism of arterioles. (**a**) A sudden increase of the intravascular pressure causes vasoconstriction and thus increases the vessel's resistance towards maintaining the flow. (**b**) A sudden pressure drop causes vasodilatation and a decreased resistance towards maintaining the flow

Blood flow-dependent regulation uses the ability of the vessel to sense WSS. The endothelium responds to WSS with the release of NO that in turn relaxes the contractile cells in the vessel wall.

The tonus of contractile vascular cells can also be controlled by other factors, such as upstream and downstream transmission of messengers along the vessel walls as well as the level of local metabolism. Regulatory messengers, manufactured and released from a site of metabolic activity, influence the activation of contractile vascular cells, especially in the wall of arterioles [548].

2.1.7.2 Short-Term Nervous Control of the Blood Pressure

Body motion and activity require the *independent* nervous control of the blood pressure for the different parts of the vascular system. Given an upright standing position for example, a gravitational shift towards the lower limbs needs to be compensated within seconds to avoid postural hypotension, also known as orthostatic hypotension. The vascular system is therefore equipped with pressure sensors that continuously record the hemodynamic regime, transduce signals, and feed the information to corresponding afferent neurons. Such receptors are called *baroreceptors* in the high-pressure circulation, and *voloreceptors* in the low-pressure circulation. Prominent baroreceptors are found in the carotid sinus and the aortic arch, whilst voloreceptors are in the pulmonary artery, the atria, the ventricles, and the vena cavae.

2.1.7.3 Long-Term Control of the Blood Pressure

The long-term control of blood pressure involves the indirect monitoring of *blood volume*. Hormonal-based control restores the blood volume and subsequently the blood pressure. The blood volume is controlled by fluid and electrolytes, such as sodium and potassium, excreted from the kidney. Other organs involved in blood volume control are the hypothalamus, sympathetic nerves, adrenal gland, and others.

2.2   Mechanical System Properties

The circulatory system relies on the pumping heart and the resistance in the vascular bed. These two effects together generated the arterial blood *pressure p* [Pa] and *flow q* [m^3 s^{-1}]—the most fundamental mechanical properties of the circulatory system. Pressure and flow appear as waves and propagate along the vascular tree.

The heartbeat forces the vascular system to oscillate and it is normally in near-periodic steady-state oscillation. Given the heart suddenly stops beating, the vascular system stops oscillating and pressure and flow decrease smoothly to zero. This is characteristic for an *over-damped system*.

Although arteries have complex geometries, in this section we consider them as long, thin-walled tubes. This 1D approximation also ignores the variation of the velocity across the cross-section, necessarily abandoning the *no-slip* condition at the wall.

2.2.1   Waves in the Vascular System

Whilst the definition of a wave is commonly linked to the specific physical phenomena it represents, waves may generally be seen as disturbances that propagate in space and time. A wave has a waveform, or profile that changes along with its propagation. The profile may be decomposed into sub-waves. Such decomposition is not unique, and historically, the most common way to represent cardiovascular waveforms is the *Fourier*[6] *decomposition*, see Appendix A.3. It treats the waveform as the superposition of sinusoidal waves at the fundamental frequency and all of its harmonics. Since Fourier analysis is carried out in the *frequency domain*, it can be difficult to relate features of the Fourier representation to specific times in the cardiac cycle.

The *wave speed c* [m s^{-1}] in the cardiovascular system is determined by the area distensibility $D = (dA/dp)/A$ [Pa^{-1}] of the vessel, and given by the relation

$$c = \frac{1}{\sqrt{\rho D}} \, , \tag{2.1}$$

---

[6]Jean-Baptiste Joseph Fourier, French mathematician and physicist, 1768–1830.

where ρ [kg m^{-3}] denotes the density of blood, and A [m^2] is the cross-section of the vessel. The derivation of (2.1) is given in Sect. 6.6.3. The waves are advected by the blood velocity v, so that the observed speed of propagation is $v + c$ in the downstream direction and $v - c$ in the upstream direction. Given normal arteries, the blood velocity v is always lower than the wave speed c.

Example 2.1 (Upstream Pressure Wave Propagation). Blood of density $\rho =$ 1060.0 kg m^{-3} is under the pressure p and flows at the velocity v in an artery of the cross-section A, see Fig. 2.9. A pressure wave propagates at the speed $c - v$ in upstream direction and changes the velocity and pressure by Δv and Δp, respectively.

Fig. 2.9 Upstream propagating of a pressure wave in a blood vessel
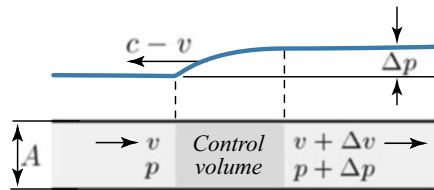
(a) Express the mass flow rate that passes through the control volume as shown in Fig. 2.9. The wave speed c in the vessel may be regarded much larger than the blood flow velocity v.
(b) Use Newton's second law of mechanics and apply it to the control volume towards the derivation of the relation between the wave speed c, the increments Δv, Δp and the blood density ρ, a relation called water hammer equation.
(c) Consider a vessel of distensibility $D = 0.0301$ kPa^{-1} and compute the wave speed c.
(d) Compute the change of velocity Δv that is caused by a pressure wave of $\Delta p = 0.23$ kPa.   ∎

Wave speed in the aorta has traditionally been determined by measuring the time it takes for the pulse wave to travel between two measurement sites—usually from the carotid to the femoral artery [394]. Although the peak of the pressure or the velocity is probably the easiest to measure, it is more accurate to measure the time of the foot of the wave. This measure alters less as the waveform changes with its propagation, and such methods are generally known as *foot-to-foot* measurements. The pressure–velocity loop provides an alternative method to measure wave speed, see Sect. 2.2.5.

The blood vessel's area distensibility D is not constant, but a function of the blood pressure, a factor that influences the wave speed (2.1). Let us consider the aorta with the aortic valve opening and closing at diastolic and late-systolic pressures, respectively. The opening and closing of the valve trigger waves that then

travel at *different* speeds along the aorta, information that may be used to identify the non-linear stress–strain property of the vessel wall properties [301].

2.2.2 Vascular Pressure

Given a position x along the vascular path, the integration over the pressure waveform $p(x, t)$ [Pa] defines the *mean pressure*

$$p_{\text{mean}}(x) = \frac{1}{T} \int_0^T p(x, t)\mathrm{d}t \approx \frac{1}{3} p_{\text{syst}}(x) + \frac{2}{3} p_{\text{diast}}(x), \tag{2.3}$$

where T [s] is the duration of a cardiac cycle, and p_{syst} and p_{diast} denote systolic and diastolic blood pressures, respectively. For practical reasons one would integrate not only over one, but a number of cardiac cycles.

The mean pressure p_{mean} continuously decreases from the aorta towards the vena cava. However, the pressure gradient is not continuous all along the vascular path but appears almost exclusively in arterioles, capillaries, and venules—the vessels of the smallest diameters, see Fig. 2.10. The *vascular bed* houses these vessels and therefore determines the resistance of the vascular system. This key role of the vascular bed has already been noticed by Hales.[7]

Aside from the mean pressure, the *pulse pressure* $p_{\text{p}} = p_{\text{syst}} - p_{\text{diast}}$ is another important hemodynamic property of the vascular system. Hales seems again to be the first to measure blood pressure and notice that pressure in the arterial system is not constant, but varies over the heartbeat. The pressure wave pulse, or waveform

Fig. 2.10 Change of pressure along the vascular path. Mean pressure p_{mean} (thick line) falls quickly at the level of the smallest vessels. The pulse pressure p_{p} (hatched area) increases towards distal arteries as a consequence of wave reflection, before it dissipates at the level of the smallest vessels. The capillaries and the entire venous system are free from pulsatility. The exchange of oxygen, nutrients, and other substances appears at the level of capillaries (gray area)

---
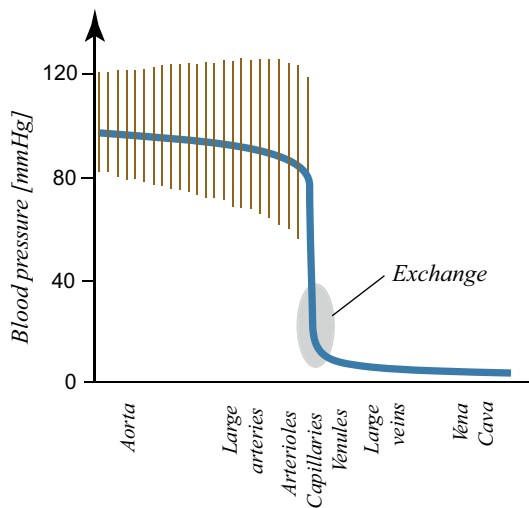
[7]Stephen Hales, English clergyman, 1677–1761.

is not only determined by the heartbeat, but it is also a direct manifestation of vascular properties. It is almost exclusively the elastic properties of the *thoracic aorta* together with the heartbeat that determines the pressure pulse.

The pressure wave travels over the arterial tree at the wave speed c, much faster than the blood flow velocity v. The vessel's distensibility and diameter determine the *wave speed* according to Eq. (2.1). The pulse wave travels two times faster in large arteries, and even four times faster in small arteries as compared to the aorta.

2.2.2.1 Pressure Waveform

A number of factors shape the pressure wave, resulting in its characteristic appearance. Fig. 2.11 illustrates the typical shape of the pressure wave in the aorta. It establishes from the superposition of the *forward* and *backward* traveling waves, see Fig. 2.11b. The forward wave originates at the ventricle, whilst the backward wave stems from wave reflections at downstream arterial branch points, where the aortic bifurcation is most dominant. The reflections explain that the pulse pressure p_p increases from the aorta towards the distal arteries and that the pressure wave looks very different in young and old subjects, see Fig. 2.11c. The aorta in old subjects is stiffer, and thus less distensible, and pressure waves travel therefore faster. The backward wave arrives then earlier and contributes more to the *systolic pressure augmentation*.

When reaching the level of arterioles, the pressure wave flattens out due to the high viscous dissipation of the flow in small vessels. Consequently, capillaries and the entire venous system are free of pulsatility, see Fig. 2.10.

2.2.3   Vascular Capacity

The *capacity* C [m^3 Pa^{-1}], also known as *volume compliance*, determines the vasculature's ability to increase the volume of blood it holds, and thus its reservoir/buffering function. Given its definition

$$C = \frac{\Delta V}{\Delta p} \, , \tag{2.4}$$

it relates the increase of blood volume ΔV [m^3] to the increase in blood pressure Δp [Pa]. The compliance, and thus the elasticity and size of the largest blood vessels determine the capacity of the vascular system.

Fig. 2.12 shows the blood volume in the arterial and venous systems as a function of the pressure [235]. The tangent to these curves is the respective capacity, and $C_{art} = 2\,\mathrm{ml\,mmHg^{-1}}$ and $C_{ven} = 100\,\mathrm{ml\,mmHg^{-1}}$ approximate the arterial and venous capacities of an adult human. The venous system stores approximately five times more blood than the arterial system and its capacity is approximately fifty times larger than that of the arterial system.

The aorta contributes almost the entire capacity to the vascular system, out of which the thoracic segment alone covers 85% [232]. The capacity of the

Fig. 2.11 The pressure pulse. (**a**) Typical pressure waveform. The systolic pressure is augmented by the backward wave. The diacrotic notch denotes the closure of the aortic valve. (**b**) The superposition of forward and backward traveling waves determines the pressure pulse. (**c**) Typical pressure waveforms in young and old subjects
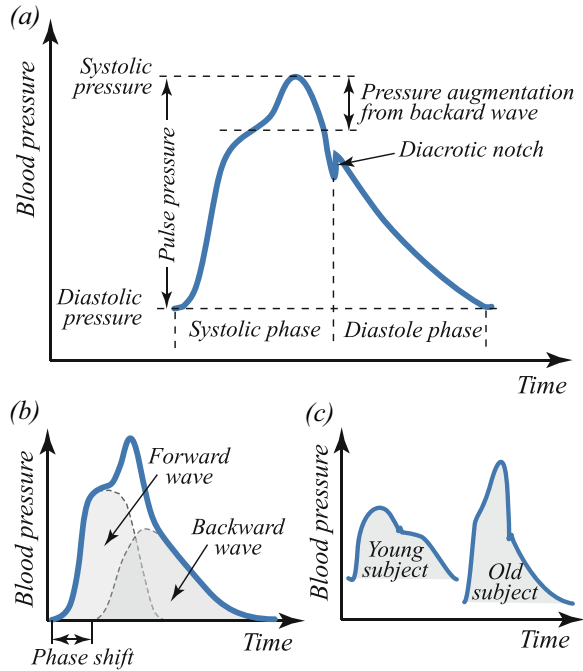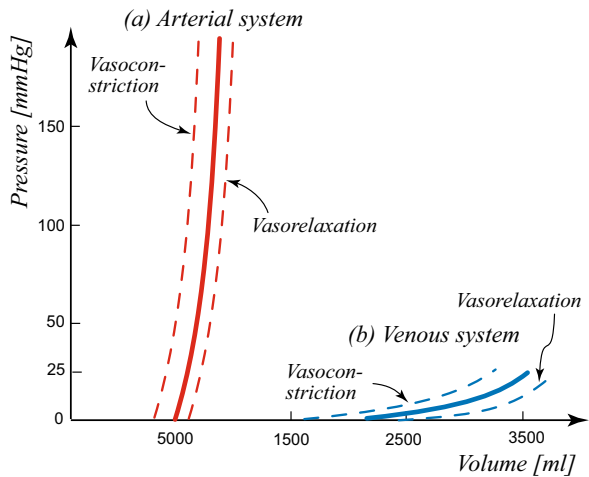
(a)

Blood pressure

Systolic pressure

Pulse pressure

Pressure augmentation from backard wave

Diacrotic notch

Diastolic pressure

Systolic phase | Diastole phase

Time

(b)

Blood pressure

Forward wave

Backward wave

Phase shift

Time

(c)

Blood pressure

Young subject

Old subject

Time

Fig. 2.12 Pressure–volume relationships of (**a**) the arterial and (**b**) the venous vascular system. Vasoreactivity influences the relationship as shown by the dashed curves

Pressure [mmHg]

(a) Arterial system

Vasocon-striction

Vasorelaxation

(b) Venous system

Vasorelaxation

Vasocon-striction

Volume [ml]

aorta is constant over a wide range of pressures and determines the circulation's *Windkessel (WK) properties*. The capacity of the aorta, and thus its elasticity, is of utmost importance to the entire cardiovascular system. A stiff aorta increases left ventricular load that may result in cardiac complications, such as cardiomyopathy. In addition to genetic or elastinopathies [94], the aorta also stiffens naturally with age. It is elastic lamellae that undergo fragmentation and thinning, leading to ectasia

and a gradual transfer of mechanical load to collagen, which is 100 to 1000 times stiffer than elastin and then reduces the capacity of the vascular system [224].

2.2.4 Vascular Flow

The aorta is the first arterial segment of the systemic circuit, directly connected to the heart. A unidirectional flow of the blood ejected from the left ventricle into the aorta is maintained through the *aortic valve*. It passively opens and closes with each heartbeat. The discontinuous inflow of blood together with the aortic capacity defines the *pulsatile blood flow* in the aorta. Given peak systole, blood flows unidirectional and at velocities of approximately $60 \, \text{cm s}^{-1}$, whilst back flow establishes at the diastolic phase. Back flow in the aortic arch and the abdominal aorta reaches velocities of approximately $-20 \, \text{cm s}^{-1}$ and $-10 \, \text{cm s}^{-1}$, respectively.

Blood flow in the large arteries is similar to the flow in the aorta. For example in the iliac artery, the velocities over the cardiac cycle range from approximately -7.5 to $60 \, \text{cm s}^{-1}$. The flow in veins is much more homogeneous as compared to arteries. Given the saphenous vein, the velocity changes only between approximately 20 and $30 \, \text{cm s}^{-1}$. The distribution of the blood flow velocity over the vessel's cross-section is complex and influenced by factors, such as the form of the pressure wave, the vessel's diameter and centerline curvature, upstream and downstream flow properties, Vortical Structure (VS) dynamics, and others. Such effects are beyond a 1D flow description and will be discussed in Chap. 6.

Flow is inverse proportional to the vasculature's cross-sectional area. At the level of the capillaries the largest cross-sectional area appears, and blood flows at velocities as low as tens of micrometers per second. A Stokes[8] flow is then an adequate model of blood flow. The very low flow velocity is important to provide enough time for the exchange of oxygen, nutrients, and other substances in the capillaries. The blood flow is linked to the vessel's biochemical activity through WSS, and changes in response to factors, such as the oxygen tension of the surrounding tissue.

Given a 1D description, the flow q and the velocity v in a vessel are related through $q = Av \, [\text{m}^3 \, \text{s}^{-1}]$, where A denotes the luminal cross-section of the vessel. Similar to the pressure $p(x, t)$, the flow $q(x, t)$ also appears as a wave in the vascular system, where x and t denote the position along the vascular path and the time, respectively.

2.2.4.1 Venous Return

Given homeostasis, the time-averaged cardiac output equals the flow into the atrium, the *venous return*. Venous return and cardiac output are therefore interdependent, a relation known as the *Frank–Starling mechanism*. In addition to factors, such as rhythmical contraction of limb muscles during normal locomotory activity, vasoreactivity, respiration, and gravitation, the (partial) collapse of veins has an

---

[8]Sir George Gabriel Stokes, English/Irish physicist and mathematician, 1819–1903.

important influence on the venous return. It appears at negative ambient pressures and has been extensively studied [259, 422]. See also Fig. 2.13 that illustrates some factors that influence venous return. At *negative* atrial pressure, veins start to collapse and the linearity between pressure and flow is broken. Venous return can then no longer increase at increasing pressure gradient, and the pressure–flow curve flattens out.

2.2.5 The Pressure–Velocity Loop

Given the pressure $p(x, t)$ and the velocity $v(x, t)$ at the position x in a vessel, the pressure–velocity loop may be plotted, see Fig. 2.14. At the beginning of the loop when the pressure and velocity waves start, the tangent to the pressure–velocity
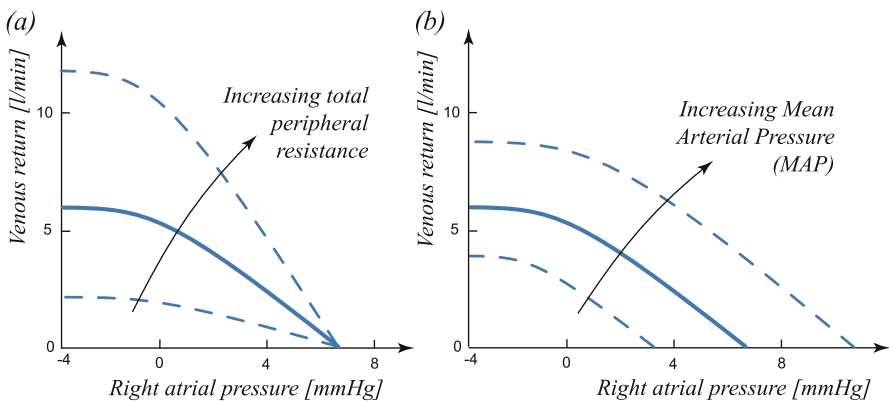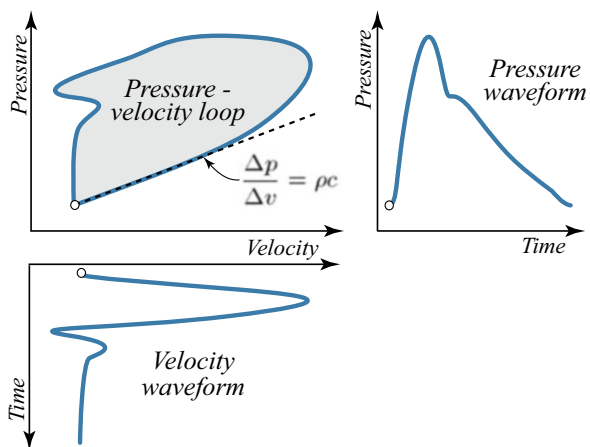

Fig. 2.13 The non-linear relation between the venous return and the atrial pressure. (**a**) Influence of the total peripheral resistance. (**b**) Influence of the Mean Arterial Pressure (MAP)

Fig. 2.14 The pressure–velocity loop illustrating the weighted wave speed ρc. The dot indicates the beginning of the pressure and velocity waves

loop expresses the weighted wave speed ρc, where ρ denotes the density of blood and c is the wave speed. The *water hammer equation* (2.2) $\Delta p / \Delta v = \rho c$ explains this property of the pressure–velocity loop, where $c \gg v$ has been assumed in the derivation of (2.2). It relates the pressure and velocity increments Δp and Δv of wave propagation and goes back to the work of von Kries,[9] and pulse wave investigations in blood vessels [571]. Given $p(x, t)$ and $v(x, t)$ can be measured accurately and simultaneously, the pressure-volume loop represents a simple and accurate method of measuring the wave speed [304].

2.2.6 Vascular Resistance

The resistance $R = \Delta p / q$ [Pa s m^{-3}] of a vessel against the flow q is expressed by the pressure drop Δp between the inlet and outlet of the segment. The viscosity of the blood and the flow conditions in the vessel determine its resistance. Given laminar steady-state tube flow, the Hagen[10]–Poiseuille[11] law expresses the hydraulic resistance, see Sect. 2.3.2.1. It states that a tube of diameter d has a resistance that is proportional to $1/d^4$, and therefore only the smallest vessels, the resistance vessels, can provide noticeable resistance to blood flow [609].

As with an individual vessel, also a network of vessels provides resistance to flow. The dimensions of the vessels together with their organization within the network then determine the resistance. The arrangement of vessels in series increases the resistance, whilst their parallel arrangement reduces the resistance. Given an adult human, $R_{art} = 1$ mmHg s ml^{-1} and $R_{ven} = 0.06$ mmHg s ml^{-1} approximate the resistances of the arterial and venous systems, respectively.

2.2.7 Transcapillary Transport

The changes of hydrostatic and osmotic pressures across the capillary wall direct the *transcapillary fluid flux*, and thus the fluid exchange between the vascular and interstitial spaces. The fluid is in principle *water* that solves proteins and electrolytes, which then is called plasma. Factors such as solute size and its electrical charge determine whether or not they can pass the semipermeable capillary wall. The fluid flux is therefore always filtrated, and the transcapillary transport is also called *filtration*. Together with the lymphatic system, filtration determines the transcapillary solute concentrations and controls interstitial (volume) homeostasis.

Whilst the muscle tonus controls the hydrostatic pressure in the microvasculature, the transcapillary solute concentrations determine the osmotic pressure. Small solutes can easily pass the capillary wall, and in most vascular beds only the

---

[9]Johannes von Kries, German physiologist, 1853–1928.

[10]Gotthilf Heinrich Ludwig Hagen, German civil engineer, 1797–1884.

[11]Jean Léonard Marie Poiseuille, French physicist, and physiologist, 1797–1869.

macromolecular solutes appear at significant different concentrations across the vessel wall. The transcapillary osmotic pressure $\Delta\Pi$ can therefore be approximated by the sum of pressure differences that are exerted by such macromolecules. *Albumin* is the most important macromolecule in this context and accounts for approximately 80% of $\Delta\Pi$.

Aside from transcapillary pressure differences, the wall's leakiness, and thus its *hydraulic conductivity* L_p [m $Pa^{-1}s^{-1}$] determines how much fluid passes through it. The conductivity is defined by Darcy's[12] law through the relation

$$L_p = \frac{k}{\eta L} \, , \tag{2.5}$$

where k [m^2] and L [m] denote the intrinsic permeability and thickness of the capillary wall, whilst η [Pa s] is the viscosity of water, see Appendix E.2. The hydraulic conductivity can also be directly measured by laboratory experiments [250].

2.3   Modeling the Macrocirculation

This section follows a top-down approach, where   *lumped parameter models* describe parts of the vascular system. They represent vascular complexity by a low number of parameters yet capturing salient system features. A topology consisting of discrete entities, representing *resistance, capacity*, and *inductance*, describes the spatially distributed vascular system. Such models do not consider the anatomical organization of the vessels and cannot represent features, such as wave propagation. Lumped parameter modeling of the vascular system is well documented with excellent reviews [596] available in the literature.

2.3.1   WindKessel Models

Whilst Weber[13] seems to be the first who proposed the comparison of the *capacity (volume compliance)* of the large arteries with the *WindKessel (WK)* present in fire engines, it was Frank[14] [173] who quantitatively formulated and popularized the so-called two-element WK model.

2.3.1.1 Two-Element WindKessel Model
The *two-element WK model* represents the systemic vascular circuit by two lumped parameters—its total *capacity* C [m^3 Pa^{-1}], and its total peripheral   *resistance* R [Pa m^{-3}], see Fig. 2.15. The capacity $C = \Delta V/\Delta p$ describes the intake of the

---

[12]Henry Philibert Gaspard Darcy, French engineer, 1803–1858.

[13]Ernst Heinrich Weber, German physician, 1795–1878.

[14]Otto Frank, German doctor and physiologist, 1865–1944.

blood volume ΔV [m^3] into the (elastic) arterial system in response to the pressure increase Δp [Pa]. In contrary, the resistance $R = \Delta p_{mean}/q_{CO}$ relates the drop of the mean pressure Δp_{mean} from the arterial side to venous side, to the cardiac output q_{CO} [m^3 s^{-1}]. Given the much higher pressure in the arterial than in the venous system, the simplification $R \approx p_{mean\,art}/q_{CO}$ may be made, where $p_{mean\,art}$ denotes the MAP. Whilst the elasticity of the aorta and the largest conduit arteries determines the system's capacity C, the resistance vessels govern the system's resistance R.

The total flow $q(t)$ through the system splits into the flow $q_R(t)$ through the resistor R and the flow $q_C(t)$ into the capacitor C, see the electrical representation of the two-element WK model in Fig. 2.15b. The flow balance then reads

$$q(t) = q_R(t) + q_C(t) = \frac{p(t)}{R} + C\frac{dp(t)}{dt}, \tag{2.6}$$

where $p(t)$ denotes the time-dependent arterial pressure, and the relations $q_R = p/R$ and $q_C = C(dp/dt)$ describe the resistor and the capacitor, see Appendix E.1. The governing equation of the two-element WK model (2.6) relates the pressure $p(t)$ and flow $q(t)$ of the systemic circuit, a system described by the properties C and R, respectively.

Given the pressure $p(t)$, relation (2.6) is an algebraic expression that directly yields $q(t)$. In contrary, given $q(t)$, it represents a first-order linear differential equation in $p(t)$ and may be solved (numerically) together with the initial condition $p(0) = p_0$. Fig. 2.16b illustrates such a (transient) solution for the pressure $p(t)$. Table 2.1 reports the systemic circuit parameters, whilst Fig. 2.16a shows

Fig. 2.15 (a) Hydraulic and (b) electric representations of the two-element WindKessel (WK) model. The flow $q(t)$ and pressure $p(t)$ describe the system state, and R and C denote vascular bed resistance and arterial capacity, respectively
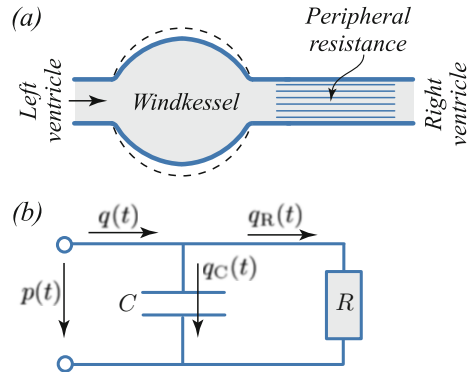
Table 2.1 System parameters used for WindKessel (WK) models

Vascular bed resistance R	1.1 mmHg s ml^{-1}
Arterial capacity C	0.7 ml mmHg^{-1}
Aortic impedance[a] Z	0.1 mmHg s ml^{-1}
Arterial inertance[b] L	0.02 mmHg s^2 ml^{-1}

[a] Only used by the three-element and four-element WK models.
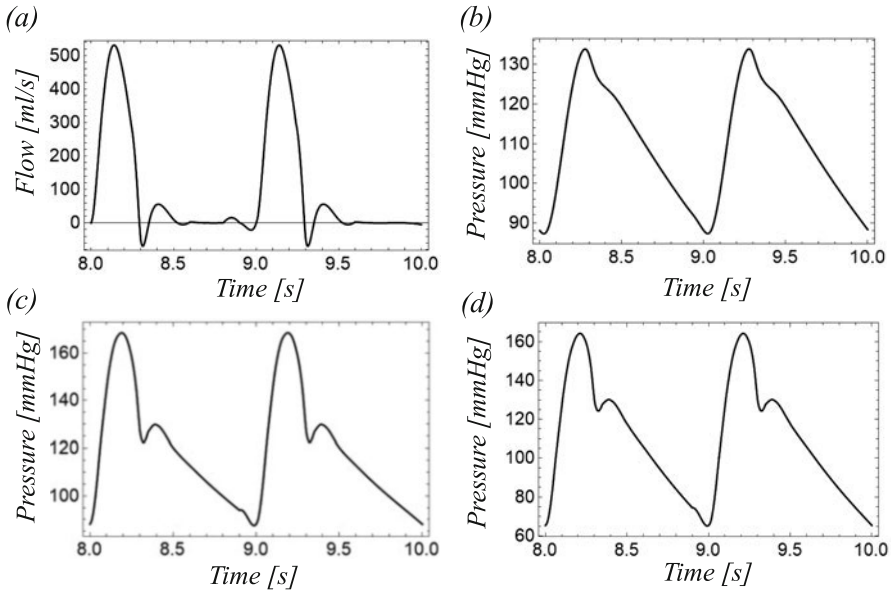[b] Only used by the four-element WK model.

Fig. 2.16 WindKessel (WK) modeling of the systemic circuit. (**a**) Prescribed flow profile $q(t)$. (**b**) Pressure profile $p(t)$ according to the two-element WK model (2.6). (**c**) Pressure profile $p(t)$ according to the three-element WK model (2.20). (**d**) Pressure profile $p(t)$ according to the four-element WK model (2.30). Table 2.1 reports the parameters used for the WK models

the prescribed flow $q(t)$ through the system. The cardiac cycle time of $T = 1.0$ s has been used, and the flow waveform was interpolated between a number of data points. The two-element WK model (2.6) has been solved at the initial condition $p_0 = 80$ mmHg, and Fig. 2.16b shows $p(t)$ for the time interval from 8.0 to 10.0 s. It is the ninth and tenth cardiac cycle, and the system has reached its steady-state periodic condition.

Example 2.2 (Two-Element Windkessel Model Predictions). A vascular system may be represented by a two-element Windkessel model, where $R = 50.1$ mmHgs ml^{-1} and $C = 0.018$ ml mmHg^{-1} describe the system's resistance and capacity, respectively. Given the cardiac cycle period $T = 1$ s, the flow

$$q(t) = \begin{cases} q_0 \sin(6\pi t) & 0 \le t \le 1/6\,\text{s}, \\ 0 & 1/6 < t < 1\text{s}, \end{cases} \tag{2.7}$$

where $q_0 = 18.2$ ml s^{-1} passes the system.

(a) Use the backward-Euler time discretization method and provide a discretized version of the two-element Windkessel model (2.6).

(b) Iteratively solve the discretized governing equation and predict the pressure $p(t)$ in the system at steady-state periodic conditions. Use different numbers k of time steps towards exploring the convergence with respect to this parameter. ∎

Example 2.3 (Systemic Implication of EVAR Treatment). Given EndoVascular Aortic Repair (EVAR), a stent-graft of diameter $d_{sg} = 2.5$ cm is inserted in the $l_{aorta} = 35$ cm long thoracic aorta to cover an aneurysm, see Fig. 2.17. The stent-graft has the radial stiffness of $k_{sg} = \Delta d/\Delta p = 1.2 \cdot 10^{-3}$ cm kPa^{-1} and covers in total 70% of the thoracic aorta. The EVAR treatment changes the capacity C of the systemic circuit, and before treatment, the capacity $C_n = 9.7$ cm^3 kPa^{-1} and the resistance $R = 0.18$ kPa s cm^{-3} determined the patient's systemic circulation.

Fig. 2.17 Schematic illustration of a thoracic aortic aneurysm that has been treated with EndoVascular Aortic Repair (EVAR). The stent-graft covers the $l_{sg} = \alpha l_{aorta}$ long aortic segment, where l_{aorta} and α denote the total length of the thoracic aorta and a dimensionless parameter, respectively
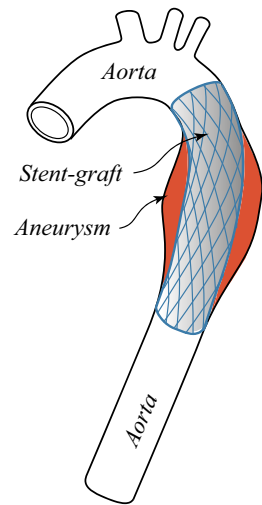
(a) Provide the relation of the capacity $C_{EVAR}(\alpha)$ as a function of the stent-graft coverage α for the EVAR-treated patient. The stent-graft coverage $\alpha = l_{sg}/l_{aorta}$ is the ratio between the stent-graft length and the length of the thoracic aorta.
(b) Consider the simplified cardiac output $q(t) = Q \sin(\pi t)^2$ with $Q = 150$ cm^3 s^{-1} and use a two-element Windkessel (WK) model to study the systemic implication of EVAR treatment. Consider the initial pressure $p(0) = 13.3$ kPa and solve the WK governing equation for $\alpha = 0$ and $\alpha = 1$, respectively. Plot the aortic pressure over the time for said parameters. The result

$$I = \int \exp(x/a) \sin^2(\pi x) dx$$

$$= \frac{a \exp(x/a) \left[1 + 4a^2\pi^2 - \cos(2\pi x) - 2a\pi \sin(2\pi x)\right]}{2 + 8a^2\pi^2} + K$$

may be used to solve the linear first-order differential equation of the WK model, where K denotes an integration constant. ∎

2.3.1.2 Homogeneous Solution

In most cases, only the *steady-state periodic, or homogenous* solution of the problem (2.6) is of interest. The analysis in the complex plane, or Argand's[15] diagram is then convenient, see Appendix A.2. The flow and the pressure are described by complex numbers, represented by the vectors **q** and **p** in the complex plane, respectively.

Let us first consider the case, where the pressure $p(t) = \text{Re}(\mathbf{p})$ is known, whilst the flow $q(t) = \text{Re}(\mathbf{q})$ through the system is unknown. At steady state, the pressure $p(t)$ (as the flow $q(t)$) is periodic and may be expressed by the Fourier series (see Appendix A.3)

$$p(t) = \text{Re}(\mathbf{p}) = \text{Re}\left(\sum_{n=-\infty}^{+\infty} \mathbf{P}_n \exp[i\omega t] \right), \tag{2.9}$$

where $\mathbf{P}_n$ and $i = \sqrt{-1}$ denote the complex Fourier coefficients and the imaginary unit, respectively. Given the additive representation (2.9) of the pressure waveform through the superposition of its harmonics, it is sufficient to consider a single complex vector $\mathbf{p} = \mathbf{P}\exp(i\omega t) = P\exp(i\omega t)$ with $P = |\mathbf{P}|$ pointing in the real direction at the time $t = 0$. With the properties of the resistor and capacitor (E.1), the governing equation (2.6) then reads

$$\begin{aligned}
\mathbf{q} &= R^{-1}P\exp(i\omega t) + iC\omega P\exp(i\omega t) \\
&= P(R^{-1} + iC\omega)\exp(i\omega t) \\
&= \mathbf{Q}\exp(i\omega t), \tag{2.10}
\end{aligned}$$

where $|\mathbf{Q}| = Q = P\sqrt{R^{-2} + C^2\omega^2}$ and $\phi = \arg(CR\omega) = \arctan(CR\omega)$ denote the *amplitude (norm)* and the *argument* of the complex flow vector $\mathbf{q}$, respectively. The time-dependent flow then reads $q(t) = \text{Re}(\mathbf{q}) = Q\cos(\omega t + \phi)$, and Fig. 2.18a illustrates it in the complex plane.

In contrary to the aforementioned analysis, we consider now the system flow $q(t)$ to be given, whilst the pressure $p(t)$ is unknown. The flow $q(t) = \text{Re}(\mathbf{q})$ may again be expressed as Fourier series $\mathbf{q} = \sum_{n=-\infty}^{+\infty} \mathbf{Q}_n \exp(i\omega t)$ with $\mathbf{Q}_n$ denoting the

---

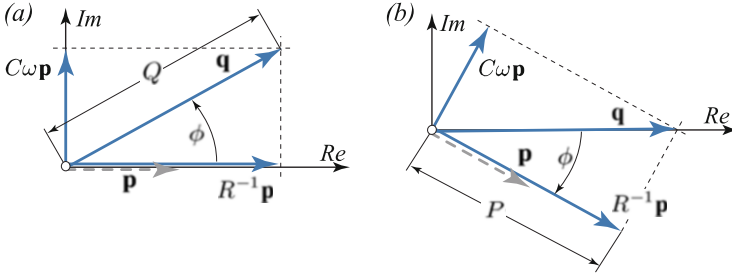[15] Jean-Robert Argand, French amateur mathematician, 1768–1822.

Fig. 2.18 Representation of flow $q(t) = \text{Re}(\mathbf{q})$ and pressure $p(t) = \text{Re}(\mathbf{p})$ in the complex plane. The relation amongst them is described by a two-element WindKessel (WK) model that describes the systemic circuit of resistance R and capacity C. (**a**) The pressure $\mathbf{p}$ is prescribed, and the WK model governs the flow $\mathbf{q}$. (**b**) The flow $\mathbf{q}$ is prescribed, and the WK model governs the pressure $\mathbf{p}$

Fourier coefficients. Again, it is sufficient to consider Eq. (2.6) for a single complex vector $q(t) = Q \exp(i\omega t)$ with $Q = |\mathbf{Q}|$ and $\mathbf{Q}$ pointing in the real direction at $t = 0$. It yields then the governing equation

$$Q \exp(i\omega t) = R^{-1} P \exp[i(\omega t + \phi)] + iC\omega P \exp[i(\omega t + \phi)]$$
$$= P \left\{ R^{-1} \exp(i\phi) + C\omega \exp[i(\phi + \pi/2)] \right\} \exp(i\omega t), \qquad (2.11)$$

where the Ansatz $p(t) = \mathbf{P}\exp(i\omega t) = P\exp[i(\omega t + \phi)]$ has been used. Whilst $P = |\mathbf{P}|$ denotes the *pressure amplitude* (norm), ϕ is the *phase angle* between pressure and flow. Both parameters need to be identified from the complex equation (2.11). Equation (2.11)$_1$ already presents real and imaginary contributions, and $P = Q/\sqrt{R^{-2} + C^2\omega^2}$ denotes the norm of the flow. Towards the specification of the phase angle ϕ, we may consider the expression (2.11) at the time $t = 0$. The flow $\mathbf{q}$ points then in the real direction, and thus the imaginary part of (2.11) vanishes. The condition

$$0 = \text{Im}\left[P \left\{ R^{-1} \exp(i\phi) + C\omega \exp[i(\phi + \pi/2)] \right\} \exp(i\omega t) \right]_{t=0}$$
$$= R^{-1} \sin\phi + C\omega \underbrace{\sin(\phi + \pi/2)}_{\cos\phi}$$

then determines $\tan\phi = -RC\omega$ to be the phase angle. Fig. 2.18b illustrates flow and pressure in Argand's diagram at the time $t = 0$ when the flow $\mathbf{q}$ points into the real direction. The governing equations (2.10) and (2.11) describe both the two-element WK model, and the vector diagrams in Fig. 2.18a,b are rotated versions of each other.
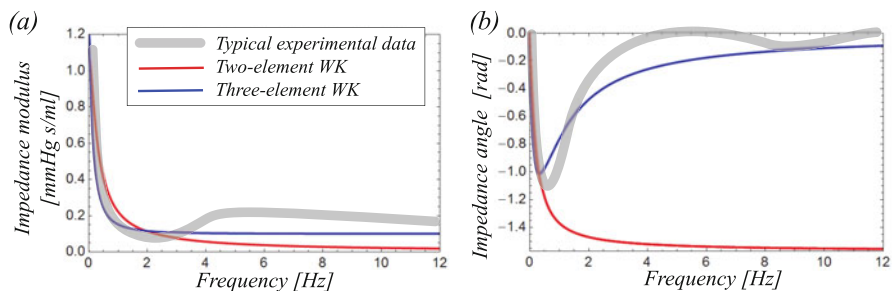
Fig. 2.19 (**a**) Impedance modulus Z and (**b**) impedance angle ϕ predicted by the two-element WindKessel (WK) (red) and the three-element WK (blue) models. The models use the parameters listed in Table 2.1, and the gray curves show typical experimental data

2.3.1.3 Impedance

The *impedance* $\mathbf{z}$ is a complex vector that relates a system's input and output. In the description of the vasculature, it compares the pressure $\mathbf{p}$ and the flow $\mathbf{q}$. The *impedance modulus* $|\mathbf{z}| = Z = |\mathbf{p}|/|\mathbf{q}| = P/Q$ [Pa s m^{-3}] is the quotient of the pressure and flow amplitudes, whilst the *impedance angle* $\phi = \arg\mathbf{q} - \arg\mathbf{p}$ [rad] is the phase difference between the two complex vectors $\mathbf{q}$ and $\mathbf{p}$, respectively. Given the flow and pressure of the two-element WK model derived in Sect. 2.3.1.2,

$$Z = (R^{-2} + C^2\omega^2)^{-1/2} \quad \text{and} \quad \phi = \arctan(RC\omega) \tag{2.12}$$

express its impedance modulus Z and angle ϕ, respectively. Fig. 2.19 shows these quantities as a function of the system frequency $f = \omega/(2\pi)$ and based on the parameters listed in Table 2.1. At steady state $f = 0$, the entire flow runs over the resistor; the system's impedance is then equal to its resistance, $Z = R$.

Example 2.4 (Impedance of the Vascular System). Table 2.2 reports measurements of aortic pressure $p(t)$ and flow $q(t)$ in the ascending ferret aorta. Given these measurements, the vascular system's impedance $\mathbf{z}$ should be computed.

(a) Provide a Fourier series approximation of $p(t)$ and $q(t)$ up to $M = 10$ harmonics. Plot the Fourier series approximation on top of the original signal.

Table 2.2 Measured flow and pressure waves in the ascending aorta of an individual ferret. Data is extracted from plots reported elsewhere [62]

Time [s]	Flow [ml s^{-1}]	Pressure [mmHg]	Time [s]	Flow [ml s^{-1}]	Pressure [mmHg]
0.0	0.00	78	0.2	0.16	90
0.0125	0.00	78	0.2125	0.20	90
0.025	0.04	77	0.225	0.30	89
0.0375	0.23	77	0.2375	0.20	87
0.05	0.48	78	0.25	0.16	86
0.0625	3.00	95	0.2625	0.13	84
0.075	4.61	97	0.275	0.10	84
0.0875	4.50	97	0.2875	0.08	83
0.1	3.96	96	0.3	0.07	82
0.1125	3.20	93	0.3125	0.06	81
0.125	2.10	90	0.325	0.06	81
0.1375	0.00	81	0.3375	0.04	80
0.15	−0.32	83	0.35	0.02	80
0.1625	−0.08	85	0.3625	0.00	79
0.175	0.14	87	0.375	0.00	78
0.1875	0.15	89			

(b) Compute the system's impedance modulus Z and impedance angle ϕ, and plot them *versus* the signal frequency f. ∎

2.3.1.4 Parameter Identification

The vascular bed's resistance R determines the relation between the mean flow q_{mean} and the mean pressure p_{mean} over the cardiac cycle. Given the time T of the cardiac cycle, the expression

$$R = \frac{p_{mean}}{q_{mean}} = \frac{\int_0^T p(t)\mathrm{d}t}{\int_0^T q(t)\mathrm{d}t} \tag{2.14}$$

allows us therefore to compute the resistance R from the flow $q(t)$ and pressure $p(t)$, respectively. The cardiovascular system is an over-damped system, and the heart directly determines its pulsatility. Therefore, $p(t)$, $q(t)$, and T may vary from cycle to cycle, and their averages over a number of cardiac cycles should be used to compute R through (2.14).

In addition to the resistance R, the capacity C of the two-element WK model needs to be identified. An approach known as *pressure decay method* considers the late diastolic phase, where the flow is approximately zero, see Fig. 2.16a. The governing equation (2.6) then reads $q(t) = p(t)/R + C\mathrm{d}p(t)/\mathrm{d}t = 0$, and the capacity

$$C = \frac{\Delta t}{R \ln \left(\frac{p_0}{p_1} \right)} \tag{2.15}$$

is given by the pressure decay over the time period $\Delta t = t_1 - t_0$. The pressures $p_0 = p(t_0)$ and $p_1 = p(t_1)$ are commonly taken at time t_0 right after the diacrotic notch, as well as at the time t_1 at the end of the diastolic phase. Alternative methods to identify C by exploring the late diastolic phase have been discussed elsewhere [596].

Example 2.5 (Decay Method to Estimate the Vascular Resistance). Given the organ's arterial capacity $C = 0.012\,\text{ml mmHg}^{-1}$, the experimental set-up shown in Fig. 2.20 is used to measure the vascular bed resistance R. At the time $t = 0$ the valve closes and stops the inflow, such that $q_{\text{in}}(t) = 0$ holds for $t > 0$. At the times $t_0 = 0.1\,\text{s}$ and $t_1 = 0.9\,\text{s}$, the manometer measures the pressures $p_0 = p_{\text{in}}(t_0) = 112.0\,\text{mmHg}$ and $p_1 = p_{\text{in}}(t_1) = 75.0\,\text{mmHg}$, respectively.
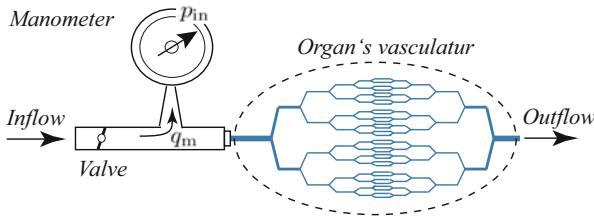

Fig. 2.20 Schematic illustration of an experimental set-up to estimate the vascular resistance R of an organ

(a) Design a lumped parameter model that represents the problem at negligible inflow $q_m = 0$ into the manometer. Derive the model's governing equation and estimate the resistance R from the two pressure measurements p_0 and p_1.
(b) Consider the flow $q_m(t) = \xi\,dp_{\text{in}}/dt$ to be proportional to the pressure change, where ξ denotes a manometer-dependent parameter. Provide the governing equation for this problem and estimate R from the two pressure measurements p_0 and p_1. Compute the relative error $e = 100(R - R_{\text{exact}})/R_{\text{exact}}$ [%] for $0 < \xi < 0.5C$, where R_{exact} denotes the resistance at $q_m = 0$.
(c) Consider the manometer to be an uptake tube with the inner diameter of $d_i = 1.0\,\text{mm}$ that is filled with water of the density $\rho = 1000.0\,\text{kg m}^{-3}$. Compute ξ for this device and estimate the resistance R of the vascular bed from the two pressure measurements p_0 and p_1. ■

Least-square parameter identification is a popular approach in the identification of model parameters. Given n measurements at the times t_i of the pressure p_i and flow q_i, the minimization problem

$$\sum_{i=0}^{n} \left[\alpha(p(R, C; t_i) - p_i)^2 + (q(R, C; t_i) - q_i)^2 \right] \to \text{MIN} \qquad (2.17)$$

allows the identification of the least-square optimized parameters R and C of the two-element WK model. Here, α denotes a scaling/weighting parameter to account for differences concerning the values of pressure and flow and to ensure that both errors contribute to the objective function. Aside from directly using the pressure and flow measurements, the impedance modulus $Z = (R^{-2} + C^2\omega^2)^{-1/2}$ and the impedance angle $\phi = \arctan(RC\omega)$ may also be used to estimate R and C. The Fourier series of the pressure and flow waves provides the pairs (Z_i, ω_i) and (ϕ_i, ω_i) for $0 \leq i \leq M$, see Example 2.4. Here, M is the number of harmonics considered by the parameter identification, whilst ω denotes the angular velocity. The minimization problem

$$\sum_{i=0}^{M} \left[\alpha(Z(R, C; \omega_i) - Z_i)^2 + (\phi(R, C; \omega_i) - \phi_i)^2\right] \rightarrow \text{MIN} \qquad (2.18)$$

allows then the identification of the least-square optimized parameters R and C, where α adjusts for data range difference.

Whilst the least-square-identified parameters yield the model that best agrees with the experimental data, the physical interpretation of R as vascular bed resistance, and C as volume compliance cannot be guaranteed.

2.3.1.5 Three-Element WindKessel Model

At higher frequencies, Fig. 2.19 demonstrates qualitative disagreement between experimental data and the predictions of the two-element WK model. Whilst the two-element WK model approaches the impedance modulus $Z = 0$ and the impedance angle $\phi = -\pi/2$ for the frequency $f \rightarrow \infty$, this is not supported by experimental data. The two-element WK model does not consider inertia effects of the blood, which is the main reason for this shortcoming.

The acceleration and deceleration of the large blood mass in the aorta influence the vascular system; it presents significant vascular resistance at higher frequencies. The *three-element WK model* introduced therefore an additional resistance $Z_a = v_{pw}\rho/A$, where v_{pw}, ρ, and A denote aortic pulse wave velocity, blood density, and aortic cross-section, respectively. The resistance Z_a is also called *aortic impedance*, and Fig. 2.21 shows the hydraulic and electric representations of the three-element WK model.

Given the flow $q(t)$ across the resistor Z_a, the pressure drops from $p(t)$ to $\overline{p}(t)$, and

$$\overline{p}(t) = p(t) - Z_a q(t) \qquad (2.19)$$

holds. In addition, the total flow splits into the part $q_R(t)$ through the resistor and the part $q_C(t)$ into the capacitor. It yields the relation

$$q(t) = q_R(t) + q_C(t) = \frac{\overline{p}(t)}{R} + C\frac{\mathrm{d}\overline{p}(t)}{\mathrm{d}t} ,$$

Fig. 2.21 (**a**) Hydraulic and
(**b**) electric representations of
the three-element WindKessel
(WK) model. Flow $q(t)$ and
pressure $p(t)$ describe the
system state, whilst R, Z_a,
and C denote the vascular bed
resistance, aortic impedance,
and arterial capacity,
respectively
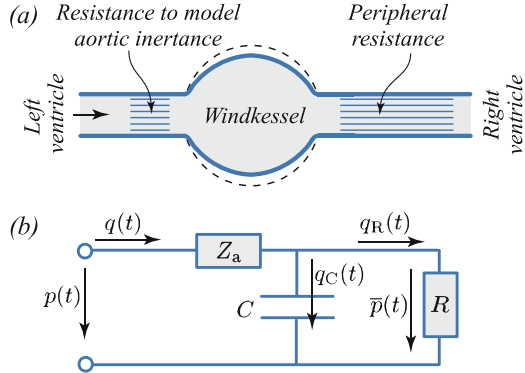
and the substitution of $\overline{p}(t)$ by (2.19) then leads to the governing equation

$$\frac{\mathrm{d}p(t)}{\mathrm{d}t} + \frac{p(t)}{RC} = Z_a \frac{\mathrm{d}q(t)}{\mathrm{d}t} + \frac{R + Z_a}{RC} q(t) \qquad (2.20)$$

of the three-element WK model. Given either $p(t)$ or $q(t)$, the relation (2.20) yields
a first-order linear differential equation. Fig. 2.16c illustrates the corresponding
(transient) solution. It is based on the prescription of the flow shown in Fig. 2.16a
and the parameters listed in Table 2.1. The solution starts at the initial condition
$p_0 = 80$ mmHg, and Fig. 2.16c shows $p(t)$ at steady-state periodic conditions.

The three-element WK model is probably the most widely used model to mimic
the vascular system. It is often realized as a test rig to test vascular medical devices.

Example 2.6 (Two-Element Versus Three-Element WK Models). Table 2.2 reports
measurements of the pressure $p(t)$ and flow $q(t)$ in the ascending ferret aorta, data
that should be used to estimate model parameters of the two-element and three-
element WK models.

(a) Estimate the peripheral resistance R of the ferret's vascular system.
(b) Estimate the total arterial capacity C of the ferret's vascular system.
(c) Estimate the ferret's aortic impedance Z_a. The aortic diameter of 6.0 mm,
    the aortic pulse wave velocity of 6.3 m s^{-1}, and the blood density of $\rho = 1060$ kg m^{-3} may be used.
(d) Prescribe the flow given in Table 2.2 and predict the pressure through the
    numerical solution of the governing equations of the two-element and three-
    element WK models. ∎

2.3.1.6 Homogeneous Solution

The steady-state periodic analysis of the problem (2.20) is conveniently investigated
in the complex plane, where the pressure and flow waves assemble from the
superposition of $\mathbf{p} = P \exp(i\omega t)$ and $\mathbf{q} = Q \exp[i(\omega t + \phi)]$, respectively. The

complex vectors **p** and **q** rotate at the angular velocity ω in the complex plane and may be seen as sub-waves, the harmonics. The phase angle ϕ between both vectors denotes the system's impedance angle. Given this Ansatz for the pressure and flow, the governing equation (2.20) yields

$$i\omega Z + \frac{Z}{CR} = i\omega Z_a \exp(i\phi) + \frac{R + Z_a}{RC} \exp(i\phi), \tag{2.21}$$

where the definition of the system's impedance modulus $Z = P/Q$ has been used.

Without loss of generality, the expression (2.21) is then investigated at the time $t = 0$ towards the identification of the system unknowns, the impedance modulus Z, and the impedance phase ϕ, respectively. Euler's[16] formula $\exp(i\phi) = \cos\phi + i\sin\phi$ allows us to split (2.21) into imaginary and real parts

$$\left.\begin{array}{l} \omega Z = \omega Z_a \cos\phi + \dfrac{R + Z_a}{RC} \sin\phi, \\[2mm] \dfrac{Z}{RC} = -\omega Z_a \sin\phi + \dfrac{R + Z_a}{RC} \cos\phi, \end{array}\right\} \tag{2.22}$$

which then results in a system with four solutions for Z and ϕ. The only physically admissible solution is

$$Z = \frac{\sqrt{\alpha\beta}}{1 + C^2 R^2 \omega^2} \;;\; \phi = \begin{cases} -\arccos\left(\dfrac{R + Z_a + C^2 R^2 \omega^2 Z_a}{\sqrt{\alpha\beta}}\right) & \omega > 0 \\[4mm] \arccos\left(\dfrac{R + Z_a + C^2 R^2 \omega^2 Z_a}{\sqrt{\alpha\beta}}\right) & \omega < 0 \end{cases} \tag{2.23}$$

with $\alpha = 2RZ_a + Z_a^2 + R^2(1 + C^2\omega^2 Z_a^2)$ and $\beta = 1 + C^2 R^2 \omega^2$.

Given the parameters listed in Table 2.1, the impedance modulus and angle (2.23) are plotted against the system frequency $f = \omega/(2\pi)$ in Fig. 2.19. The three-element WK qualitatively captures the experimental observations, and at high frequencies the system's impedance approaches the aortic impedance $Z \to Z_a$. At steady state $f = 0$, the entire flow passes the total resistance $R + Z_a$, and the system's impedance then is $Z = R + Z_a$.

Example 2.7 (Impedance-Based Estimation of WK Parameters). A ferret vascular system has a cardiac cycle of $T = 0.375$ s, and Table 2.4 shows its impedance **z** up to the frequency f of approximately 10 Hz. Given this information, the parameters of the two-element and three-element WK models should be identified through least-square optimization.

(a) Define an objective function Φ and identify the least-square-optimized model parameters. Given the two-element WK model, the optimization problem $\Phi(R, C; \omega) \to \text{MIN}$ determines the resistance R and the capacity C. Given

---

[16]Leonhard Euler, Swiss mathematician, physicist, astronomer, logician and engineer, 1707–1783.

Table 2.4 Impedance modulus Z and impedance angle ϕ of an individual ferret vascular system, see also Example 2.4

Frequency	Impedance modulus [mmHg s ml^{-1}]	Impedance angle [rad]
0.00000	108.415	0.00000
2.66667	4.12022	−0.96618
5.33333	3.34739	0.172411
8.00000	5.01376	0.132572
10.6667	4.60703	0.056390

Table 2.5 Fourier coefficients of a cyclic flow wave $q(t)$ with the period of $T = 0.375$ s

Frequency [Hz]	Fourier coefficients [ml s^{-1}]
0.00000	0.786333
2.66667	$0.0276938 - 0.646413\,i$
5.33333	$-0.555816 - 0.112961\,i$
8.00000	$-0.0896779 + 0.408525\,i$
10.6667	$0.216635 + 0.0557698\,i$

the three-element WK model, the optimization problem $\Phi(R, C, Z_a; \omega) \to$ MIN determines the resistance R, the capacity C, and the characteristic aortic impedance Z_a.

(b) Plot the impedance modulus Z and impedance angle ϕ as predicted by the WK models on top of the data given in Table 2.4.

(c) Consider the flow wave $q(t)$ represented by the Fourier coefficients in Table 2.5 and compute the WK model-predicted pressure $p(t)$. Use a steady-state periodic analysis and compare the pressure with the predictions of a transient analysis. The numerical solution of the WK governing equations over a sufficiently large number of cardiac cycles, may be used.   ∎

2.3.1.7 Four-Element WindKessel Model

Whilst the three-element WK model is suitable for many applications, the physical interpretation of the aortic impedance may be questioned [527]. Motivated by this shortcoming, the *four-element WK model* includes the *total arterial inertance* as an *inductor* element L in the circuit, see Fig. 2.22. It influences the system only at low frequencies.

The total flow $q(t)$ splits into the flow q_R through the vascular bed resistor R and the flow q_C into the capacitor C and determines the relation

$$q(t) = q_R + q_C = \frac{\overline{p}(t)}{R} + C\frac{\mathrm{d}\overline{p}(t)}{\mathrm{d}t} . \tag{2.26}$$

Fig. 2.22 (**a**) Hydraulic and
(**b**) electric representations of
the four-element WindKessel
(WK) model. Flow $q(t)$ and
pressure $p(t)$ describe the
system state. The model
parameters R, Z_a, C and L
denote vascular bed
resistance, aortic impedance,
arterial capacity, and total
arterial inertance, respectively
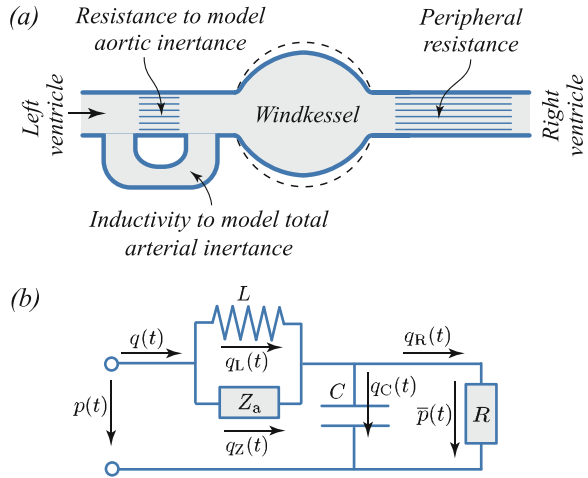
Given the flow $q_Z(t)$ over the aortic impedance Z_a, the total pressure $p(t)$ drops
and

$$\bar{p}(t) = p(t) - Z_a q_Z(t) \tag{2.27}$$

holds. The pressure drop over Z_a is equal to the pressure drop over the inductor L,

$$L\frac{\mathrm{d}q_L}{\mathrm{d}t} = Z_a q_Z(t), \tag{2.28}$$

where $p - \bar{p} = L(\mathrm{d}q_L/\mathrm{d}t)$ has been used to describe the inductor element, see
Appendix E.1. The flow $q_L(t)$ and the flow $q_Z(t)$ together determine the total system
flow

$$q(t) = q_L(t) + q_Z(t), \tag{2.29}$$

which then closes the mathematical description of the four-element WK model.

The four equations (2.26)–(2.29) form the system

$$\left.\begin{aligned}
\frac{\mathrm{d}p(t)}{\mathrm{d}t} + \frac{p(t)}{CR} &= Z_a\frac{\mathrm{d}q_Z(t)}{\mathrm{d}t} + \frac{Z_a}{RC}q_Z(t) + \frac{q(t)}{C}, \\
\frac{\mathrm{d}q_Z(t)}{\mathrm{d}t} &= \frac{\mathrm{d}q(t)}{\mathrm{d}t} - \frac{Z_a}{L}q_Z(t),
\end{aligned}\right\} \tag{2.30}$$

of linear differential equations that governs the four-element WK model. The
expressions (2.26) and (2.27) lead to the first statement, whilst the second one
follows from (2.28) and the time derivative of (2.29).

Given either $p(t)$ or $q(t)$, the system (2.30) may be solved numerically, and Fig. 2.16d illustrates such a (transient) solution. It considers the flow shown in Fig. 2.16a and uses the parameters listed in Table 2.1. The solution starts at the initial condition $p_0 = 80$ mmHg, and Fig. 2.16d shows $p(t)$ at steady-state periodic conditions.

## 2.3.2 Vessel Network Modeling

Lumped parameter models may also be used for the analysis of a *network of vessels*. Such a model facilitates the exploration of how changes in one part of the network influence the pressure $p(t)$ and flow $q(t)$ somewhere else in the network. They may therefore test the outcome of vascular interventions, for example. A lumped parameter model expresses the pressure and flow as functions of the time t and neglects their dependence on the vascular path coordinate x—a network model can therefore not simulate phenomena, such as wave propagation.

Given a network of n vessel segments, the individual segments are represented by their *capacity C_i*, *resistance R_i*, and *inertance L_i*; $i = 1, \ldots, n$, and then connected at m network nodes. Different designs of lumped parameter models have been proposed to describe the biomechanics of a vessel segment. The *three-element vessel model* illustrated in Fig. 2.23 is one possible design. It models a vessel segment of diameter d [m], length l [m], and wall thickness h [m], which is entirely filled by blood of the density ρ [kg m^{-3}] and the dynamic viscosity η [Pa s].

2.3.2.1 Vessel Segment Resistance
A laminar, steady-state and fully developed flow in a cylindrical vessel results in a *parabolic velocity profile* over the vessel's cross-section called a Poiseuille flow. The WSS that develops in response to the fluid flowing over the vessel wall presents resistance to the flow q. Given Poiseuille flow, the flow q and WSS τ_{w} are related through $q = -r^3 \pi \tau_{\mathrm{w}}/4$, where r denotes the vessel radius, see Chap. 6.

Fig. 2.23 (**a**) Schematic and (**b**) electric representations of the three-element vessel model. The flows $q_{\mathrm{in}}(t)$, $q_{\mathrm{out}}(t)$ and the pressures $p_{\mathrm{in}}(t)$, $p_{\mathrm{out}}(t)$ describe vessel inlet and outlet conditions. The vessel's biomechanical properties are expressed by its capacity C, resistance R, and inertance L, respectively
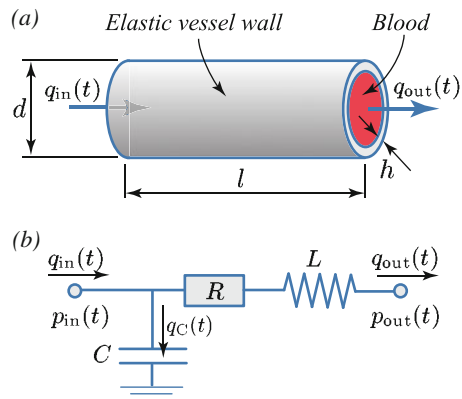
The flow q through the vessel depends on the pressure drop Δp between the vessel's inlet and outlet, and

$$R = \frac{\Delta p}{q} = \frac{128\eta l}{\pi d^4} \qquad (2.31)$$

determines the *resistance* R against flow, a relation known as the *law of Hagen–Poiseuille*. Poiseuille flow provides a good description in smaller vessels and veins, whilst in large arteries the blood flow is highly influenced by inertia effects. A parabolic velocity profile is then only present during the systolic phase of the cardiac cycle, see Chap. 6.

The vessel's resistance R represents energy dissipation, and in addition to (2.31), dissipative sources may also relate to unsteady flow, flow separation, vessel curvature, and vessel bifurcations [376]. Finally, we note that laboratory experiments may also be used for the direct measurement of the resistance R of a vessel.

2.3.2.2 Vessel Segment Capacity

The vessel segment's *capacity* expresses the increase ΔV of blood volume that is inside the vessel in response to the increase Δp in pressure. This property can either be measured experimentally or predicted through the modeling of the elasticity of the vessel wall. Given linear elasticity, or Hooke's[17] law in the description of the vessel wall,

$$C = \frac{\Delta V}{\Delta p} = \frac{3d^3\pi l}{16hE} \qquad (2.32)$$

expresses the vessel's capacity, where E [Pa] denotes the vessel wall's Young's[18] modulus, see Sect. 3.5.2. We may also derive the alternative expression (5.2) that considers any non-linear elastic description of the vessel wall.

2.3.2.3 Blood Inertance

Given the mean blood flow velocity $v_{mean} = q(t)/A$, the force equilibrium of the blood segment along the axial direction reads $\Delta p A = -\rho A l \dot{v}_{mean}$, where the contribution from WSS has been neglected. It allows us to express the pressure increment $\Delta p = \rho l \dot{q}/A$ as a function of the change of flow $\dot{q}$, where the cross-section $A = d^2\pi/4$ was assumed to be constant along the vessel. The *inertance*

$$L = \frac{\Delta p}{\dot{q}} = \frac{4\rho l}{d^2\pi} \qquad (2.33)$$

then describes the inertia of the blood in the vessel.

---

[17]Robert Hooke, English natural philosopher, architect, and polymath, 1635–1703.
[18]Thomas Young, English polymath and physician, 1773–1829.

Example 2.8 (Renal Artery Adaptation to Partial Nephrectomy). Figure 2.24 schematically illustrates the surgical removal of a part of the kidney, an intervention called partial nephrectomy. It increases the kidney's vascular bed resistance R by the factor α. At baseline the renal artery has the radius r_0 and wall thickness h_0, properties that alter in response to the intervention towards r and h, respectively. Homeostasis drives the adaptation, and r and h change until the renal artery's Wall Shear Stress (WSS) τ_w as well as its circumferential wall stress σ_θ return to their homeostatic values. It may be assumed that the arterial pressure and blood properties are not influenced by the surgical intervention.

Fig. 2.24 Schematic illustration of partial nephrectomy, with the dark area indicating the removed section of the kidney
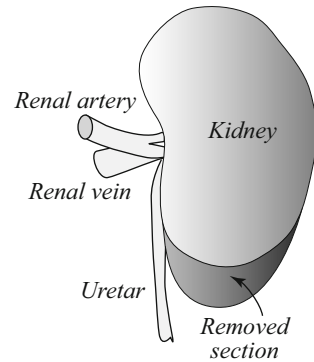
(a) Derive the relation between the factor α that augments the resistance and the mean flow q through the kidney.
(b) Assume Poiseuille flow and derive the relation between the WSS τ_w and the mean flow q through the renal artery.
(c) Express the circumferential wall stress σ_θ as a function of vessel's dimensions and the blood pressure. Consider the thickness of the vessel to be much smaller than its diameter.
(d) At homeostatic conditions of τ_w and σ_θ, r/r_0 and h/h_0 should be expressed as functions of α. ∎

2.3.2.4 Governing Equation
Each lumped parameter model of a vessel has its specific governing equation, and this section discusses the design shown in Fig. 2.23. The sum of the pressure drop Δp_R over the resistance as well as Δp_L over the inertance, determines the total pressure change

$$p_{in} - p_{out} = \Delta p_R + \Delta p_L = R q_{out} + L \dot{q}_{out} , \tag{2.37}$$

where p_{in} and p_{out} denote the pressure at the vessel inlet and outlet, respectively. The flow continuity

$$q_{in} - q_{out} = q_C = C\dot{p}_{in} \tag{2.38}$$

closes the mathematical description, and in the derivation of (2.37) and (2.38) the properties of circuit elements have been used, see Appendix E.1. The model also assumes a negligible ambient (interstitial) pressure, and the capacity C is therefore directly exposed to the inlet pressure p_{in}.

Equations (2.37) and (2.38) may be rearranged towards

$$p_{out} = p_{in} - R(q_{in} - C\dot{p}_{in}) - L(\dot{q}_{in} - C\ddot{p}_{in}),$$

$$q_{out} = q_{in} - C\dot{p}_{in},$$

which then expresses the relation between input and output by the matrix equation

$$\begin{bmatrix} p_{out} \\ q_{out} \end{bmatrix} = \begin{bmatrix} 1 & -R \\ 0 & 1 \end{bmatrix} \begin{bmatrix} p_{in} \\ q_{in} \end{bmatrix} + \begin{bmatrix} RC & -L \\ -C & 0 \end{bmatrix} \begin{bmatrix} \dot{p}_{in} \\ \dot{q}_{in} \end{bmatrix} + \begin{bmatrix} LC & 0 \\ 0 & 0 \end{bmatrix} \begin{bmatrix} \ddot{p}_{in} \\ \ddot{q}_{in} \end{bmatrix}. \tag{2.39}$$

In symbolic notation it reads

$$\mathbf{d}_{out} = \mathbf{K}\mathbf{d}_{in} + \mathbf{D}\dot{\mathbf{d}}_{in} + \mathbf{M}\ddot{\mathbf{d}}_{in}. \tag{2.40}$$

The set $\{p, q, \dot{p}, \dot{q}, \ddot{q}\}$ of state variables describe the system, and a time-marching algorithm may be used to solve the governing equation (2.40) at prescribed boundary and initial conditions.

We may for example consider a *backward-Euler* discretization over the time step Δt, and the first and second time derivatives are then approximated by

$$\left.\begin{aligned} \dot{x}_{in} &= \frac{x_{in} - x_{in\,n}}{\Delta t} = \frac{x_{in}}{\Delta t} - \frac{x_{in\,n}}{\Delta t}, \\ \ddot{x}_{in} &= \frac{\dot{x}_{in} - \dot{x}_{in\,n}}{\Delta t} = \frac{x_{in}}{\Delta t^2} - \frac{x_{in\,n}}{\Delta t^2} - \frac{\dot{x}_{in\,n}}{\Delta t}, \end{aligned}\right\} \tag{2.41}$$

where $x = p, q$ and $(\bullet)_n$ denotes a quantity at the previous time step. Given such a discretization, the system (2.40) of differential equations leads to the algebraic set of equations

$$\begin{bmatrix} p_{out} \\ q_{out} \end{bmatrix} = \begin{bmatrix} 1 + \frac{RC}{\Delta t} + \frac{LC}{\Delta t^2} & -R - \frac{L}{\Delta t} \\ -\frac{C}{\Delta t} & 1 \end{bmatrix} \begin{bmatrix} p_{in} \\ q_{in} \end{bmatrix} + \mathbf{H}, \tag{2.42}$$

where the *history vector*

$$\mathbf{H} = \begin{bmatrix} -\frac{RC}{\Delta t} - \frac{LC}{\Delta t^2} & \frac{L}{\Delta t} \\ \frac{C}{\Delta t} & 0 \end{bmatrix} \begin{bmatrix} p_{in\,n} \\ q_{in\,n} \end{bmatrix} - \begin{bmatrix} \frac{LC}{\Delta t} & 0 \\ 0 & 0 \end{bmatrix} \begin{bmatrix} \dot{p}_{in\,n} \\ \dot{q}_{in\,n} \end{bmatrix}, \tag{2.43}$$

stores information from the previous time step. Consequently, the system (2.42) uniquely specifies the relation between input and output variables.

Example 2.9 (Two-Element Vessel Segment Model).   An arterial vessel segment of the resistance R and the capacity C is modeled by the lumped parameter model shown in Fig. 2.25. The model is used for a steady-state periodic analysis of a vascular network.
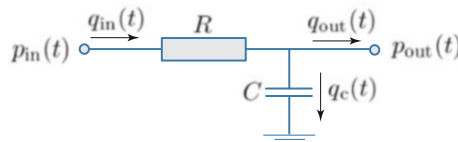
Vessel diameter d	5.2 mm
Vessel segment length l	12.7 cm
Vessel wall thickness h	0.5 mm
Vessel wall Young's modulus E	34.0 kPa
Dynamic blood viscosity η	4.0 mPa s

Fig. 2.25 Electrical representations of a two-element vessel model with the corresponding vessel segment parameters. The flows $q_{in}(t)$, $q_{out}(t)$ and the pressures $p_{in}(t)$, $p_{out}(t)$ describe the vessel inlet and outlet conditions. The vessel's biomechanical properties are expressed by the capacity C and resistance R, respectively

(a) Derive the governing equations of the lumped parameter model shown in Fig. 2.25 and rearrange them according to the system of equations

$$\begin{bmatrix} \mathbf{p}_{out} \\ \mathbf{q}_{out} \end{bmatrix} = \begin{bmatrix} K_{11} & K_{12} \\ K_{21} & K_{22} \end{bmatrix} \begin{bmatrix} \mathbf{p}_{in} \\ \mathbf{q}_{in} \end{bmatrix} + \begin{bmatrix} D_{11} & D_{12} \\ D_{21} & D_{22} \end{bmatrix} \begin{bmatrix} \dot{\mathbf{p}}_{in} \\ \dot{\mathbf{q}}_{in} \end{bmatrix},$$

where $\mathbf{p}_{in}$, $\mathbf{q}_{in}$ and $\mathbf{p}_{out}$, $\mathbf{q}_{out}$ are complex vectors that describe the inlet and outlet, respectively.

(b) Given the data in Fig. 2.25, compute the resistance R and the capacity C of the vessel segment.

(c) Compute the flow and pressure in the vessel in response to the cyclic boundary conditions $\mathbf{p}_{out} = |\mathbf{p}_{out}| \exp[i(\omega t + \pi/6)]$ and $\mathbf{q}_{in} = |\mathbf{q}_{in}| \exp[i\omega t]$, where $|\mathbf{p}_{out}| = 12.5$ Pa and $|\mathbf{q}_{in}| = 4.3$ ml s^{-1} are the pressure and flow amplitudes, whilst $\omega = 73\pi$ denotes the angular velocity of the imaginary vectors. Use Argand's diagram to draw pressure and flow in the complex plane.   ∎

Example 2.10 (Three-Element Vessel Segment Model). The lumped parameter model in Fig. 2.26 uses the resistance R, the capacity C, and the inductance L to describe an arterial vessel segment.
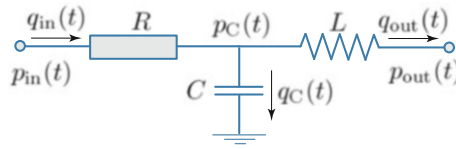
Resistance R	$2.22223 \cdot 10^6$ Pa s m^{-3}
Capacity C	$7.12003 \cdot 10^{-10}$ m^3 Pa^{-1}
Inductivity L	$6.1846 \cdot 10^6$ Pa s^2 m^{-3}

Fig. 2.26 Electrical representations of a three-element vessel model with vessel segment parameters. The flows $q_{in}(t)$, $q_{out}(t)$ and the pressures $p_{in}(t)$, $p_{out}(t)$ describe vessel inlet and outlet conditions. The vessel's biomechanical properties are expressed by the resistance R, capacity C, and inductance L, respectively

(a) Derive the governing equations of the lumped parameter model shown in Fig. 2.25 and rearrange them according to

$$\mathbf{d}_{out} = \mathbf{K}\mathbf{d}_{in} + \mathbf{D}\dot{\mathbf{d}}_{in} + \mathbf{M}\ddot{\mathbf{d}}_{in} \,,$$

where $\mathbf{d}_{out} = [p_{out}\, q_{out}]^{\mathrm{T}}$ denotes the outlet condition, whilst $\mathbf{d}_{in} = [p_{in}\, q_{in}]^{\mathrm{T}}$, $\dot{\mathbf{d}}_{in} = [\dot{p}_{in}\, \dot{q}_{in}]^{\mathrm{T}}$ and $\ddot{\mathbf{d}}_{in} = [\ddot{p}_{in}\, \ddot{q}_{in}]^{\mathrm{T}}$ describe the inlet conditions.

(b) Compute the flow and pressure for the steady-state periodic inflow $\mathbf{q}_{in} = |\mathbf{q}_{in}| \exp[i\omega t]$ with $|\mathbf{q}_{in}| = 4.3$ ml s^{-1} and $\omega = 2\pi$, and against the constant outlet pressure $\mathbf{p}_{out} = |\mathbf{p}_{out}| = 1000.0$ Pa. Use Argand's diagrams to illustrate the magnitude and phase angle of each complex quantity. ∎

2.3.2.5 Assembly of Vessel Networks

Vessel segment models, such as the three-element model described by Eq. (2.40), may be connected at *nodes* to form a network of vessels. The *compatibility conditions* relate then the flow q and the pressure p (and their time derivatives) across network nodes. Given a single vessel connects to another single vessel, the compatibility condition at the node simply reads $q_1 = q_2$ and $p_1 = p_2$ with the index denoting the vessel number.

Given a single vessel that bifurcates into two vessels, the compatibility condition reads $q_1 = \xi_q q_2 + (1 - \xi_q)q_3$ and $p_1 = p_2 = p_3$, where the index denotes the vessel number. The system state variable $0 \leq \xi_q \leq 1$ describes how the flow splits in the bifurcation, and identical to the other state variables, ξ_q is identified by the solution of the system of equations that represents the entire network of vessels. It might also be required to consider a *pressure drop* at network nodes to capture *energy dissipation* from significant flow disturbance at the bifurcation. The pressure compatibility conditions then read $p_1 = \xi_p p_2$. Here, $0 \leq \xi_p \leq 1$ accounts for the pressure drop, and p_1 and p_2 denote the pressure upstream and downstream the bifurcation, respectively.

Example 2.11 (Connected Vessel Segments). Figure 2.27 illustrates the connection of three vessels and their properties. The inflow $q_{in} = q_0[1 + \sin(\omega t)]$ with $q_0 = 0.05$ ml s^{-1} and $\omega = 2\pi$ is prescribed, whilst the constant pressures $p_2 = 11.5$ kPa and $p_3 = 11.0$ kPa are applied at the outlets. The vessels are filled with blood of the density $\rho = 1060$ kg m^{-3} and the dynamic viscosity $\eta = 3.5$ mPa s.

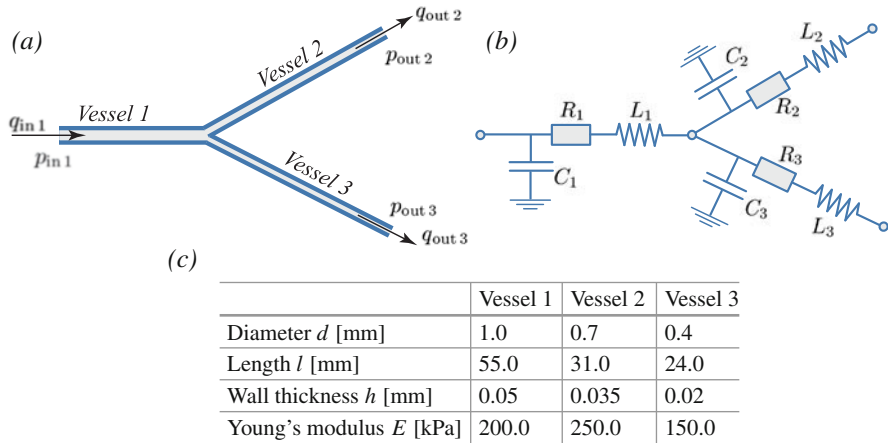|	Vessel 1	Vessel 2	Vessel 3
Diameter d [mm]	1.0	0.7	0.4
Length l [mm]	55.0	31.0	24.0
Wall thickness h [mm]	0.05	0.035	0.02
Young's modulus E [kPa]	200.0	250.0	150.0

Fig. 2.27 (**a**) Schematic and (**b**) electrical representation of a lumped parameter model that represents three connected vessel segments (**c**) Geometrical and mechanical properties of vessel segments

(a) Compute the resistance R_i, the capacity C_i, and the inductance L_i of the three vessels $i = 1, 2, 3$.

(b) Derive the governing equation of the i-th vessel according to the lumped parameter model shown in Fig. 2.27b.

(c) Provide incremental governing equations of the connected vessels by considering the time derivatives of flow and pressure according to the backward-Euler discretization (2.41).

(d) Propose an algorithm for the iterative solution of the incremental governing equations. At the bifurcation a dissipation-free flow may be considered, and the factor $0 \leq \xi \leq 1$ determines the flow split.

(e) Plot the pressure at the inlet $p_{in\,1}(t)$, the flows at the outlets $q_{out\,1}(t)$, $q_{out\,2}(t)$ as well as the flow split factor $\xi(t)$ over the time. ∎

2.4   Modeling the Microcirculation

This section describes models towards the analysis of exchange aspects in the micro-circulation. They are limited to passive microfluidic transport mechanisms, and a bottom-up approach aims at modeling the physics of microcirculatory exchange. Exchange models are well documented with excellent reviews [40, 338, 493] available in the literature.

2.4.1   Transcapillary Concentration Difference

The vessel wall of capillaries may be seen as a rigid porous body that is perforated by a large number of micro-channels connecting the vessel lumen with the interstitial space. The transport of *substances or solutes* through such micro-channels determines the transcapillary concentration difference of a solute. Towards the analysis of this property, we consider a micro-channel of length L filled with fluid that contains a solute at the concentration $c(x)$ [mol m^{-3}], where $0 \leq x \leq L$ denotes the Cartesian coordinate along the micro-channel, and thus across the capillary wall. Given microvascular exchange, the fluid is essentially *water*.

Diffusive and *advective* transport govern the *solute flux* J_s [mol s^{-1}m^{-2}] along the micro-channel. At steady state, J_s is constant all along the channel and governed by the first-order partial differential equation

$$J_s = \text{const} = \underbrace{-D \, \text{grad} c(x)}_{\text{Diffusion}} + \underbrace{c(x)v}_{\text{Advection}} \quad , \qquad (2.48)$$

where v [m s^{-1}] denotes the transport velocity of solute particles, whilst D [m^2 s^{-1}] is the diffusion constant for solute particles in water. Towards a dimensionless analysis, we may introduce $\xi = x/d$ and normalize the solute particle path length x with the solute particle diameter d. Equation (2.48) has then the solution $c(\xi) = J_s/v + H \exp(\xi Pe)$, where $Pe = vd/D$ and H denote the Péclet[19] number and an integration constant, respectively.

The Péclet number is the ratio between advective and diffusive transport. At large Péclet numbers the solvent moves together with the fluid flow, whilst at low numbers it moves independently from the motion of the fluid. The solute particles may not be spherical, and d then denotes the Stokes diameter—the diameter of the hydrodynamically similar, but spherical particle.

The aforementioned integration constant H can be identified from the solute concentration c_v in the vascular space, and thus at the inlet of the micro-channel. The solute concentration then reads $c(\xi) = J_s/v + \exp(\xi Pe)(c_v - J_s/v)$. We may also introduce the interstitial solute concentration $c_i = c(\xi = L/d)$, such that

---

[19] Jean Claude Eugène Péclet, French physicist, 1793–1857.

$$J_s = c_v v - \frac{v \Delta c}{\exp[Pe(L/d)] - 1} \tag{2.49}$$

finally expresses the solute flux across the capillary wall, where $\Delta c = c_i - c_v$ is the transcapillary concentration difference.

At steady state, the interstitial solute concentration c_i depends on the transcapillary filtration flux q_f [m s^{-1}] that determines the flow rate across the unit area of the capillary wall, see Sect. 2.4.2. Experimental data suggest that c_i is proportional to the solute flux J_s but inverse proportional to the filtration flux q_f [543]. It therefore justifies the relation $c_i = J_s/q_f$ and allows for the substitution of J_s in (2.49). The transcapillary concentration difference then reads [370]

$$\Delta c = c_v - c_i = \sigma c_v \frac{\exp[Pe(L/d)] - 1}{\exp[Pe(L/d)] - \sigma}, \tag{2.50}$$

where the solute particle velocity $v = (1-\sigma)q_f$ has been related to the filtration flux q_f through Staverman's[20] osmotic reflection coefficient σ [526], see Appendix E.3.

Example 2.12 (LDL Transport Through a Micro-channel). Low-Density Lipoprotein (LDL) is a protein of about 25 nm in size and transports fat molecules around the body. Increased LDL concentration has been strongly associated with the development of atherosclerosis—LDL that invades the vessel wall is oxidized and then poses a risk for the development of atherosclerosis. Endothelial Cells (EC) junctions form micro-channels, and LDL eventually slowly "leaks" across the endothelial barrier into the vessel wall. The model system shown in Fig. 2.28 may be used to investigate LDL transport through EC junctions.
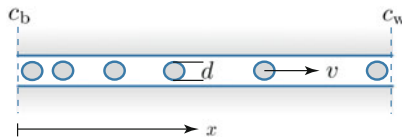

Fig. 2.28 Transport of Low-Density Lipoprotein (LDL) of diameter d and velocity v through a micro-channel. LDL concentrations in the bloodstream and the arterial wall are denoted by c_b and c_w, respectively

(a) Consider the velocity $v = q_f(1 - \sigma)$ of the LDL particles and express the LDL flux. Here, $q_f = 1.0\ \mu m\ s^{-1}$ and $\sigma = 0.78$ denote the fluid velocity and Staverman's osmotic reflection coefficient, respectively.
(b) Plot the LDL flux at the Péclet numbers $Pe = 0.01; 0.1; 1.0$ and the boundary concentrations of $c_b = 2.0\ mol\ m^{-3}$ and $c_w = 0.1\ mol\ m^{-3}$. ∎

---

[20] Albert Jan Staverman, Dutch chemist, 1911–1993.

2.4.2   Filtration

Filtration is the transport of water through the capillary wall in response to *hydrostatic* and *osmotic* pressure differences. From the vascular space to the interstitial space, the hydrostatic pressure falls from p_v to p_i, whilst COP increases from Π_v to Π_i. The exchange of water between the two spaces is determined by the *filtration flux q_f* [m s^{-1}], and thus the flow rate that passes through the unit area of wall, see Appendix E.2. Given the flow through the vessel wall is aligned with the vessel's radial direction, the flux q_f is identical to the flow velocity.

2.4.2.1 Starling's Filtration Model

Filtration in the microvasculature may be described by Starling's filtration model [524]

$$q_f = L_p \left(\Delta p - \sigma \Delta \Pi \right) \ , \tag{2.51}$$

where $\Delta p = p_v - p_i$ is the transcapillary hydrostatic pressure, whilst $\Delta \Pi = \Pi_v - \Pi_i$ denotes the transcapillary COP. The term $\Delta p - \sigma \Delta \Pi$ is called *net filtration pressure* and positive for flow from the vascular system into the interstitium. In (2.51), L_p [m Pa^{-1}s^{-1}] and σ denotes the capillary wall's hydraulic conductivity and its Staverman's osmotic reflection coefficient [526], respectively. Whilst the hydraulic conductivity describes the leakiness of the wall to water, the reflection coefficient σ corrects the theoretical COP difference to match the effective one, see Appendices E.2 and E.3.

According to (2.51), the filtration is governed by the four "Starling forces" p_v, p_i, $\sigma \Pi_v$, and $\sigma \Pi_i$. The model is also "symmetric"—the increase in p_v (or Π_v) or the decrease of p_i (or Π_i) by the same amount affects the flux equally.

2.4.2.2 Predicted Exchange

The net effect from the inflow and outflow of water across the capillary walls determines the exchange in the vascular bed. The direct measurement of exchange is difficult, and a model, such as Starling's filtration law (2.51), helps to interpret (incomplete) experimental data.

The linear relation between q_f and Δp has been shown in a population of vessels [321], whilst much less experimental data confirmed the linearity between q_f and $\Delta \Pi$ [417]. The development of flow requires the hydrostatic pressure p_v to decrease along the vascular tree. Given human nailfold skin capillaries, pressures of $p_v = 35$ to 45 mmHg at the arterial side and $p_v = 12$ to 15 mmHg at the venous sides have been reported [322]. In addition, the interstitial hydrostatic pressure $p_i = -4$ to 0 mmHg is slightly below the atmospheric pressure in many tissues, and $\Pi_v = 25$ to 28 mmHg is believed to represent vascular COP in humans. Table 2.9 summarizes this information, and Starling's law (2.51) then predicts the fluid exchange that is shown in Fig. 2.29.

Table 2.9 Representative parameters for the description of a number of soft biological tissues

Hydrostatic pressure in the capillary p_v	Arterial/venous side: 35.0/12.0 mmHg
Hydrostatic pressure in the interstitium p_i	-2.0 mmHg
Colloid Osmotic Pressure (COP) in the capillary Π_v	Arterial/venous side: 28.0/25.0 mmHg
COP in the interstitium Π_i	1.0 mmHg
Hydraulic conductivity of the capillary wall L_p	$1.5 \cdot 10^{-9}$ m s^{-1}mmHg^{-1}
Reflection coefficient of the capillary wall σ	1.0

Fig. 2.29 Exchange of fluid along capillaries. (**a**) Transcapillary hydrostatic pressure Δp and transcapillary Colloid Osmotic Pressure (COP) $\Delta\Pi$. (**b**) Filtration flux q_f across the capillary wall. Exchange according to Starling's filtration model (2.51) and the data listed in Table 2.9. (**c**) Net outward flux at the arterial side and net inward flux at the venous side
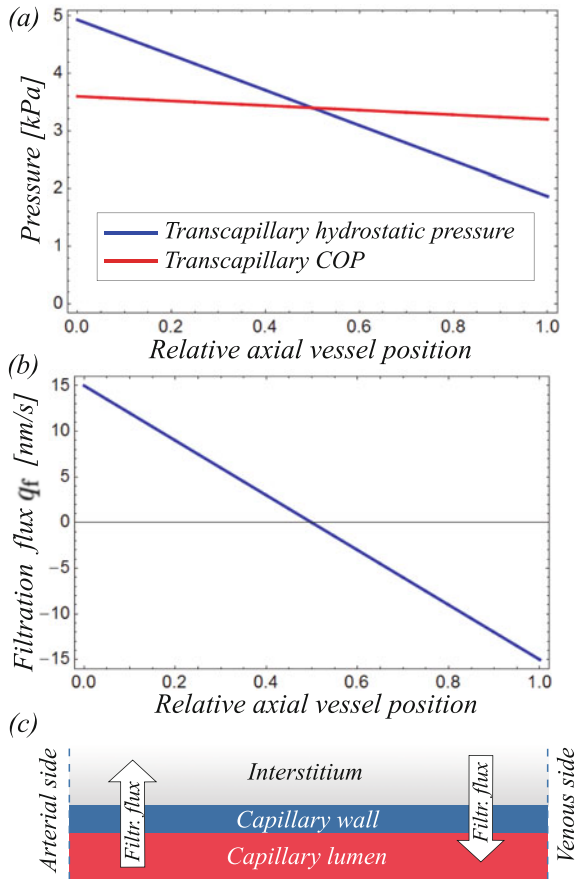

These findings suggest the exchange mechanism proposed by Starling in 1896 [524]: fluid transport into the interstitial over the arterial half of the capillary where $\Delta p > \sigma\Delta\Pi$, and reabsorbtion over the venous half where $\Delta p < \sigma\Delta\Pi$, see Fig. 2.29c. At transient conditions this mechanism has been confirmed by more advanced experiments [371], but counter-evidence emerged in a number of tissues

at steady-state exchange conditions. A revised understanding of vascular exchange is presented in Sect. 2.4.2.3.

Example 2.13 (Transport Across the Ascending Vasa Recta Wall). The model system shown in Fig. 2.30 should be used to investigate the exchange of solutes between the Ascending Vasa Recta (AVR) of the renal medulla and its interstitial space. The AVR segment is $L = 1.2$ mm long, has a diameter of $D = 29\,\mu$m, and blood flows through it at the rate $q = 35$ nl min^{-1}.

Fig. 2.30 Model system to investigate the exchange between the Ascending Vasa Recta (AVR) and the interstitium
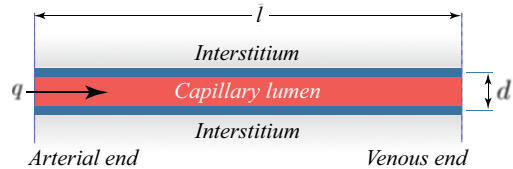
(a) Compute the distribution of the hydrostatic pressure p_v along the AVR segment. Blood may be regarded as a Newtonian fluid with the dynamic viscosity $\eta = 3.5$ mPa s, and the pressure $p_{v\,art} = 7.8$ mmHg applies at the AVR's arterial end.
(b) Compute the exchange along the AVR according to Starling's filtration law. Within the interstitium, the hydrostatic pressure $p_i = 6.0$ mmHg and the Colloid Osmotic Pressure (COP) $\Pi_i = 3.7$ mmHg are given. In addition, COP changes linearly from $\Pi_{v\,art} = 26.0$ mmHg at the arterial end to $\Pi_{v\,ven} = 16.7$ mmHg at the venous end. The Staverman's osmotic reflection coefficient $\sigma = 0.78$ and the hydraulic conductivity $L_p = 1.5 \cdot 10^{-9}$ m s^{-1}mmHg^{-1} may be assumed in the description of the vessel wall.   ∎

2.4.2.3 Current Understanding of Microvascular Exchange

Filtration measurements in response to a sudden change of the capillary hydrostatic pressure p_v [371] challenged the aforementioned concept of microvascular exchange. The filtration experiment recorded *transient results* right after the pressure step as well as *steady-state results* at least 2 min after it. Whilst the transient results confirmed earlier experiments [417], and once again validated the linearity between q_f and the transcapillary hydrostatic pressure Δp_v, the steady-state results did not show such a linearity and therefore contradicted Starling's filtration law (2.51). The observed slight imbalance in the transcapillary hydrostatic pressure at steady state favors a positive net filtration pressure. The fluid moves therefore into the interstitial space and is then *almost exclusively* drained via the lymphatics. Given the interstitial fluid volume remains constant, the filtration flux times capillary surface is equal to lymph flow. Whilst such steady-state exchange is observed in many tissues, the net filtration pressure is also negative in some tissues [338]. It then facilitates the function of organs, such as the kidney and intestinal mucosa. The lion part of the interstitial fluid is then absorbed back into the vascular compartment.

2.4.2.4 Colloid Osmotic Pressure

The macromolecule *albumin* is the main contributor to the COP in the vasculature. In the vascular space the albumin concentration remains approximately constant, and transcapillary COP is therefore primary controlled by the *interstitial* albumin concentration.

Given albumin's transcapillary concentration Δc_{alb}, Hoff's[21] law relates it to the transcapillary COP

$$\Delta \Pi_{\mathrm{alb}} = \phi \overline{R} \theta \Delta c_{\mathrm{alb}} , \qquad (2.53)$$

where the universal gas constant $\overline{R} = 8.3145 \text{ J K}^{-1}\text{mol}^{-1}$, the absolute temperature θ [K], and the osmotic coefficient ϕ have been introduced, see Appendix E.2. Albumin is a relatively small protein and passes the capillary wall together with water, and Δc_{alb} develops according to transport discussed in Sect. 2.4.1. Given (2.50) and (2.53), the transcapillary albumin COP may therefore be expressed by

$$\Delta \Pi_{\mathrm{alb}} = \sigma \, \Pi_{\mathrm{v\,alb}} \frac{\xi - 1}{\xi - \sigma} \; ; \; \xi = \exp[Pe(L/d_{\mathrm{alb}})] , \qquad (2.54)$$

where d_{alb} and L are the albumin's Stokes diameter and the capillary wall thickness, respectively. In addition, $\Pi_{\mathrm{v\,alb}} = \phi \overline{R} \theta c_{\mathrm{v\,alb}}$ is the albumin's COP in the vascular space, whilst $Pe = (1 - \sigma)q_{\mathrm{f}}d_{\mathrm{alb}}/D$ is the Péclet number with D [$\text{s}^{-1}\text{m}^{-1}$] denoting albumin's diffusion constant in water. The calculation of Pe assumes that albumin moves at the velocity $v = (1 - \sigma)q_{\mathrm{f}}$ across the capillary wall, where σ and q_{f} denote Staverman's osmotic reflection coefficient and the filtration flux, respectively. Equation (2.54) may easily be adapted to proteins other than albumin.

2.4.2.5 The Non-linear Filtration Law

Albumin is the main contributor to osmosis in the microcirculation, and $\Delta \Pi$ in Starling's filtration model (2.51) may therefore be approximated by (2.54), which then yields the relation

$$q_{\mathrm{f}} = L_{\mathrm{p}} \left[\Delta p - \sigma^2 \Pi_{\mathrm{v\,alb}} \frac{1 - \xi}{1 - \sigma\xi} \right] \; ; \; \xi = \exp[Pe(L/d_{\mathrm{alb}})] . \qquad (2.55)$$

Given the Péclet number $Pe = (1 - \sigma)q_{\mathrm{f}}d_{\mathrm{alb}}/D$, the expression (2.55) is implicit in the filtration flux q_{f}. Fig. 2.31 plots it against the transcapillary hydrostatic pressure Δp, where the properties in Table 2.10 have been used. The plot illustrates the *non-linearity* between q_{f} and Δp. It is caused by the second term at the right side of Eq. (2.55)$_1$ and determines the *diffusion-related* contribution to Δp. Diffusion is only significant at small Péclet numbers, whilst at high Péclet numbers, this term

---

[21] Jacobus Henricus van 't Hoff, Jr., Dutch physical chemist, 1852–1911.

Fig. 2.31 Filtration flux q_f in relation to transcapillary hydrostatic pressure Δp, as predicted by the non-linear filtration model (2.55). At high positive Δp, the vessel's hydraulic conductivity L_p determines exchange, whereas almost no flux appears at negative Δp
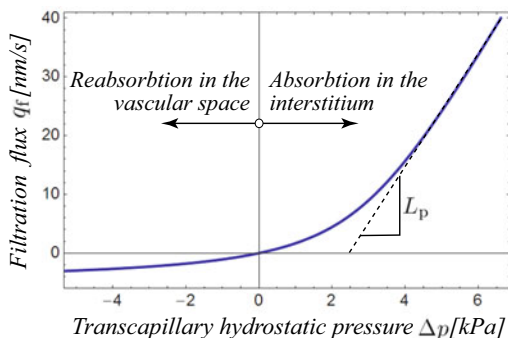

Transcapillary hydrostatic pressure Δp[kPa]

Table 2.10 Set of parameters used in the non-linear filtration model (2.55)

Diffusion coefficient D for albumin in water	$1.0 \cdot 10^{-14}\,\mathrm{m^{-2}s^{-1}}$
Thickness of the capillary wall L	$2.0 \cdot 10^{-6}\,\mathrm{m}$
Colloid Osmotic Pressure (COD) in the vascular space $\Pi_{v\,alb}$	$28.0\,\mathrm{mmHg}$
Hydraulic conductivity of the capillary wall L_p	$1.5 \cdot 10^{-9}\,\mathrm{m\,s^{-1}mmHg^{-1}}$
Staverman's osmotic reflection coefficient σ	0.95

vanishes, and the relation between q_f and Δp is fully determined by the hydraulic conductivity L_p of the wall. The curve in Fig. 2.31 is therefore linear at high transcapillary hydrostatic pressures.

The non-linear filtration model (2.55) holds for steady-state conditions—given enough time for the albumin concentration to settle down, steady-state conditions establish, and the assumptions made to derive (2.54) hold.

Fig. 2.31 shows minimal reabsorption back into the vascular space, conditions that holds for most, but not all tissues. In the kidney and the intestinal mucosa, interstitial fluid is continuously renewed by protein-free fluid, which in turn breaks the dependence of the filtration flux and the solute concentration. The assumptions made to derive equation (2.54) are then not valid, and fluid flux is best predicted by Starling's filtration model (2.51).

2.4.2.6 Two-Pore Models

The filtration flux (2.55) suggests minimal reabsorption at the venous side of capillaries [338], which is confirmed by experimental data in many tissues [371]. The lack of reabsorption backs into the vascular system, making it difficult to reconcile with low *in vivo* values for whole-body lymph flow rates. A class of models, known as *two-pore models*, aim at resolving this shortcoming [464]. Whilst albumin is not amongst the largest proteins, it still cannot pass the capillary wall through most pores. Most fluid flux q_f occurs through small pores that hinder albumin transport, whilst large pores that support the advection of albumin transport only a minute fraction of water through the wall.

The glycocalyx–cleft model illustrated in Fig. 2.32 is a specific case of a two-pore model. It assumes that the glycocalyx, *not* the entire capillary wall, dominates the filtration properties and represents the effective osmotic barrier. The glycocalyx almost entirely determines the reflection coefficient σ and the transcapillary COP. The COP underneath the glycocalyx layer is therefore very low, which in turn yields levels of net filtration fluxes that would compare to reported lymph drainage rates.

Example 2.14 (Glycocalyx–Cleft Model). Starling's filtration model (2.51) over-predicts the filtration flux q_f and has therefore been further developed towards the glycocalyx–cleft model shown in Fig. 2.32. The glycocalyx layer presents a system of ultra-fine pores in series to the larger pores formed by the endothelial clefts and thus the spaces between adjacent Endothelial Cells (ECs). Given the strong washout of albumin upon the filtration flux through the endothelial clefts, albumin concentration c_{gc} becomes very low underneath the glycocalyx layer. Along the filtration path three distinct albumin concentrations therefore establish: c_v in the vascular space, c_{gc} underneath the glycocalyx layer, and c_i in the interstitial space, see Fig. 2.32.

Given a $L = 3.5$ mm long capillary, which wall has the hydraulic conductivity of $L_p = 2.3 \cdot 10^{-9}$ s^{-1}mmHg^{-1}m and the Staverman's osmotic reflection coefficient $\sigma = 0.8$, the glycocalyx–cleft model should be analyzed. In addition, the hydrostatic pressure $p_i = -1.0$ mmHg and the Colloid Osmotic Pressure (COP) $\Pi_i = 3.7$ mmHg are approximately constant in the interstitium. Given the vascular space, the hydrostatic pressure changes linearly from $p_{v\,art} = 9.4$ mmHg to $p_{v\,ven} = 6.7$ mmHg, and the COP from $\Pi_{v\,art} = 15.8$ mmHg to $\Pi_{v\,ven} = 13.9$ mmHg between the capillary's arterial and venous ends, respectively.
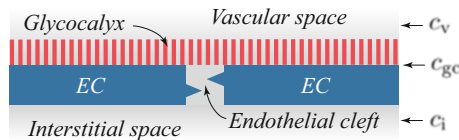

Fig. 2.32 Schematic illustration of the glycocalyx–cleft model. The glycocalyx layer provides a system of ultra-fine pores in series to the larger pores formed by the Endothelial Cell (EC) clefts

(a) Compute the fluid flux q_f across the capillary wall according to Starling's filtration model (2.51).
(b) Given $c_{gc} = (1 - \alpha)c_v + \alpha c_i$ describes the albumin concentration underneath the glycocalyx layer, compute the fluid flux q_f according to the glycocalyx–cleft model for $\alpha = 1.0; 0.9; 0.8$. ∎

2.5   Summary and Conclusion

Following the introduction of circulatory physiology, this chapter introduced a number of concepts and models towards the exploration of vascular mechanisms and system responses. The models have been either 1D in space or time, or the combination of both dimensions then led to 2D problem descriptions. Such approaches are simple and *very effective* in the investigation of how system parameters interact and influence vascular physiology and pathology. We assumed that key vasculature properties can be described by parameters, such as resistance, capacity, and hydraulic conductivity. Complex vascular mechanisms have therefore been lumped into key system parameters towards the description of *surrogate vascular functions*. The introduced system parameters can either be directly measured by tailored experiments or indirectly identified through parameter calibration methods.

The cardiovascular system is equipped with a large number of hemodynamic regulation mechanisms towards diverting blood flows and optimally perfusing the body [548]. It has also been hypothesized that in health homeostasis, a *functional crosstalk* between central and peripheral segments of the circulation is required for optimal operation [9]. This communication may be compromised, and a vicious cycle of minute alterations in central arterial stiffness and peripheral resistance starts, leading to the dramatic changes in arterial properties observed in response to diseases and aging—the mother of all diseases.

Whilst the modeling approaches discussed in this chapter fit a number of vascular applications, they may often fail to provide in-depth explanations of how local physical mechanisms determine and alter vascular parameters and function. In addition, the analysis of vascular biomechanical problems may require a multi-dimensional space-time description of individual vessel segments. This is clearly beyond the ability of the approaches discussed in this chapter, and the remaining parts of this book concerns tools and models for the analysis of individual vessel segments. It allows us then to explore localized vascular phenomena to further our understanding of vascular function. The up-scaling or homogenization of local vessel properties determines then the surrogate system parameters used in the present chapter. The generalized distributed lumped parameter framework recently reported [376] would be such an example. It allows one to compute the flow and pressure dynamics in blood vessels upon various sources of energy dissipation mechanisms.